Erschienen in: RSC Advances ; 4 (2014), 5. - S. 2447-2465
https://dx.doi.org/10.1039/C3RA44909B

RSC Advances

REVIEW

View Article Online
View Journal | View Issue

Fluorescence correlation spectroscopy in polymer science

Cite this: *RSC Adv.*, 2014, **4**, 2447

Dominik Wöll*[ab]

Fluorescence correlation spectroscopy (FCS) is a well-established technique for studying dynamic processes and interactions with minimal invasion into the corresponding system. Even though FCS has been mainly applied to biological systems, within the last 15 years an increasing number of studies in material sciences have appeared, demonstrating its enormous potential also for this field. Apart from investigations on colloidal systems, polymer science has benefited significantly from this technique. This review will summarize FCS studies on polymer systems and, in particular, focus on the diffusion of differently sized molecular and macromolecular probes in polymer solutions, classical and responsive polymer gels, polymer melts and glasses. It will be discussed how FCS can be used to determine translational and rotational diffusion in polymer solutions and at interfaces, scaling laws, micellization and aggregation and, to some extent, polymer structure including heterogeneity. Thus, FCS should be considered a powerful complement to other methods for the investigation of polymer structure and dynamics.

Received 5th September 2013
Accepted 5th November 2013

DOI: 10.1039/c3ra44909b

www.rsc.org/advances

Polymers have emerged as the most important materials of the modern world. The reason for their success lies in the variety of functions they can cover due to their tunable properties. A faceted knowledge of how these properties are determined by the structure and dynamics on different length scales is still amongst the scientists' dreams. The complexity of this relationship challenges all experimental and theoretical methods, and only combining their strengths will allow us to gain a consistent picture of polymers from the nanoscopic to the macroscopic scale.

Within the last 15 years, fluorescence correlation spectroscopy (FCS) has significantly contributed to the insights into polymer systems, in particular to diffusion measurements. Even though the first paper on FCS by Magde, Webb and Elson was already published in 1972,[1] several developments were necessary to exploit the power it has reached today.[2–7] One major step in the evolution of FCS was its combination with confocal microscopy which allows for enhanced spatial resolution and sensitivity.[8] Further important improvements concern the quality of optical components, the sensitivity and time-resolution of detectors, and better labels and labelling strategies. The advantages of FCS are (i) small sample consumption, (ii) negligible dye concentration and thus perturbance of sample properties, (iii) the possibility of *in situ* measurements, (iv) good spatial resolution at the diffraction limit and (v) the possibility to observe diffusion of different species depending on their fluorescence labelling. The majority of FCS studies have been conducted in biological systems. Transferring the concepts and technical knowledge gained in these studies to polymer science, however, is straight-forward.

In this review, I will report on FCS studies in polymer systems and how this modern technique contributed to new insights in polymer structure and dynamics. The review starts with an introduction to fluorescence correlation spectroscopy covering theoretical and technical aspects of diffusion measurements, their possibilities, limitations and pitfalls. In the next section, I briefly report on diffusion of polymer chains

[a]*Zukunftskolleg, University of Konstanz, Universitätsstr. 10, 78464 Konstanz, Germany*
[b]*Department of Chemistry, University of Konstanz, Universitätsstr. 10, 78464 Konstanz, Germany. E-mail: dominik.woell@uni-konstanz.de; Tel: +49 7531 88 2024*

Dominik Wöll received his diploma in chemistry from the University of Konstanz (Germany) in 2002 and finished his PhD at the same university in 2006, working with Prof. Ulrich E. Steiner on intramolecular sensitization of photolabile protecting groups for DNA chip synthesis. After a postdoctoral stay with Prof. Johan Hofkens at the KU Leuven (Belgium) where he became acquainted with single molecule spectroscopy techniques, he started an independent junior research group as fellow of the Zukunftskolleg of the university of Konstanz in 2008. His current research focus is single molecule fluorescence spectroscopy and microscopy in soft matter.

in pure solvents, followed by an extended section on diffusion of molecular and macromolecular probes in polymer solutions, gels, melts and glasses. In the end of that section, I will also briefly review how the diffusion of large nanoparticles can probe microrheology in polymer systems and, furthermore, report on FCS studies in responsive hydrogels and at solid–liquid interfaces, and demonstrate the power of this method to study micellization and aggregation.

I will concentrate on synthetic polymers neglecting the impressive results on biopolymers, such as dynamics[9–13] and hybridization[14–16] of DNA, polysaccharides,[17–21] protein binding and dynamics,[22–28] motor proteins,[29,30] fibrin polymerization,[31] enzyme kinetics,[32] diffusion through meshes formed by semi-rigid biopolymers,[33] and polymer–membrane interaction.[34] It will be also not further discussed how FCS can assist in analysing the photokinetics in conjugated polymers,[35] or detect molecular mobility at interfaces,[36,37] nor will this review cover FCS studies performed with nanoparticles.[38–44] With respect to the latter topic, I refer to the review on FCS studies in the journal "Current Opinion in Colloid & Interface Science" by Koynov *et al.*[45]

Fluorescence correlation spectroscopy

Basics of fluorescence correlation spectroscopy

In the following, the basic principles of FCS will be summarized. In a typical FCS experiment, as shown in Fig. 1, a collimated laser beam is focused by an objective lens into a diffraction limited confocal volume within the sample placed on a glass coverslip. Part of the light emitted from this confocal volume is collected by the same objective and separated from excitation light using a dichroic mirror and an emission filter. The emission light is focused onto a pinhole blocking most of the light not originating from the confocal volume, thereby improving the axial z-resolution as shown in Fig. 2. The confocal volume typically amounts to *ca.* 0.1 femtolitre. The photons passing through the pinhole are detected with an avalanche photo diode (APD). Such APDs possess good quantum efficiencies and, with appropriate electronics, allow for the determination of the arrival times of single photons with an accuracy in the picosecond range.

Typically, the arrival times are binned and an autocorrelation function $G(\tau)$ calculated over the resulting time traces of the intensity $I(t)$ or its deviations $\delta I(t) = I(t) - \langle I(t)\rangle$ from the mean intensity:

$$G(\tau) = \frac{\langle \delta I(t)\cdot \delta I(t+\tau)\rangle}{\langle I(t)\rangle^2} = \frac{\langle I(t)\cdot I(t+\tau)\rangle}{\langle I(t)\rangle^2} - 1 \qquad (1)$$

The autocorrelation function contains information on all processes which cause intensity fluctuations within the confocal volume. Such processes are translational and rotational diffusion or photophysical or photochemical transformations of the fluorescent probes such as transitions to the triplet state. Due to the large span in time scales of these different processes, the time axis of the autocorrelation function is often represented in a logarithmic scale.

In the following paragraph, I will concentrate on translational diffusion. As the fluorescent probe enters or leaves the confocal volume, it causes fluctuations which can be typically observed as a drop in the autocorrelation in the millisecond to second range. The autocorrelation is described by the following function[2]

$$G(\tau) = \frac{1}{N}\left(1+\frac{\tau}{\tau_D}\right)^{-1}\left(1+\left(\frac{w_{xy}}{w_z}\right)^2\frac{\tau}{\tau_D}\right)^{-\frac{1}{2}} \qquad (2)$$

where N is the number of independently diffusing dye molecules in the confocal volume, τ_D is the average diffusion time of the probes through the confocal volume with the radial and the axial diameter w_{xy} and w_z, respectively. Typical values are *ca.* 300 nm for w_{xy}, and *ca.* 1.5 μm for w_z. The square root term in

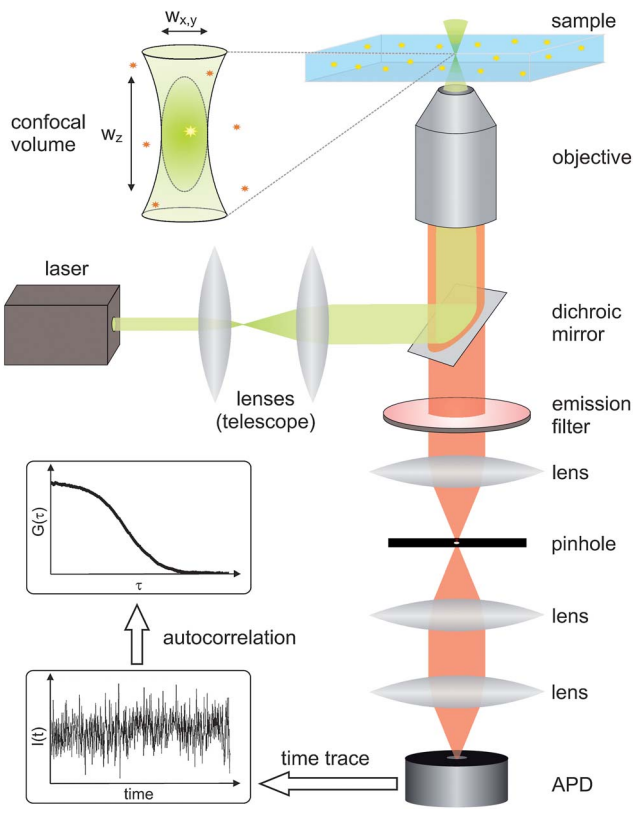

Fig. 1 Typical FCS setup as described in the text.

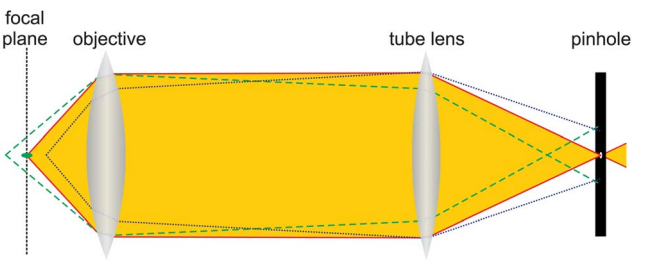

Fig. 2 Effect of the pinhole on the axial resolution of a confocal microscope. Only light originating from the focal plane (red solid line, orange area) can pass the pinhole without loss. Light from other planes (green dotted line and blue dotted line) is mainly blocked.

eqn (2) accounts for the ellipsoid shape of the confocal volume.

The highest sensitivity for the determination of τ_D is realized when in average approx. one independently diffusing probe molecule is present in the confocal volume, *i.e.* at sub-nanomolar concentrations. For much higher concentrations, the changes in intensity caused by probes entering and leaving the confocal volume have to be detected against an intensity background limiting the sensitivity of determining τ_D. As obvious from eqn (2), a high value of N results in a low autocorrelation which often cannot be fitted appropriately. On the other hand, if the probe concentration is too low, the events of a probe diffusing through the confocal volume become rather seldom. In this case, too, a fit of eqn (2) to the noisy autocorrelation curves will fail if the time traces are not recorded for a sufficiently long period.

The diffusion coefficient D can be calculated from the diffusion time using Einstein's equation for the mean square displacement in two dimensions (the third dimension is accounted for by the square root expression in eqn (2)):

$$D = \frac{{w_{xy}}^2}{4\tau_D} \tag{3}$$

The width w_{xy} of the confocal volume can be determined with a reference measurement. For aqueous systems, a common and reliable reference is rhodamine 6G (Rh6G) in water with a diffusion coefficient of 4.14×10^{-10} m^2 s^{-1}.[46] The referencing for non-aqueous systems is challenging and will be discussed later in this article. For statistically independent, freely diffusing fluorescent probes, the temporal evolution of the mean square displacement $\langle r^2(\tau)\rangle$ has been calculated from the autocorrelation function $G(\tau)$:[9]

$$G(\tau) = \frac{1}{N}\left(1 + \frac{2\langle r^2(\tau)\rangle}{3{w_{xy}}^2}\right)^{-1}\left(1 + \frac{2\langle r^2(\tau)\rangle}{3{w_z}^2}\right)^{-\frac{1}{2}} \tag{4}$$

The applicability of this formula has been disputed recently and might not be given for all cases.[47–49]

Fitting the autocorrelation curve with only one diffusion time is often not sufficient. Apart from optical misalignment which should be carefully ruled out, this can originate from size distributions of the fluorescent probes, introduced *e.g.* by a polymerization process resulting in labelled polymer chains with a non-negligible polydispersity, aggregation of dyes or labelled particles, or diffusional heterogeneities on a length scale relevant for FCS. All of these cases will cause bad fits of the autocorrelation function with eqn (2). Thus, one can start to introduce two or more (n) terms with the average number N_i of molecules of the diffusing species i and its relative fluorescence yield α_i to fit the autocorrelation according to[6,50,51]

$$G(\tau) = \frac{\sum_{i=1}^{n} N_i \cdot {\alpha_i}^2 \cdot \left(1 + \frac{\tau}{\tau_{D_i}}\right)^{-1}\left(1 + \left(\frac{w_{xy}}{w_z}\right)^2 \frac{\tau}{\tau_{D_i}}\right)^{-\frac{1}{2}}}{\left(\sum_{i=1}^{n} N_i \cdot \alpha_i\right)^2} \tag{5}$$

with each additional free parameter improving the fit, often however without obtaining additional physical information. Instead, if one molecular species diffuses in different environments bearing different diffusion coefficients but a constant fluorescence yield, it often makes more sense to obtain diffusion time distributions. This requires solving the ill-posed problem of calculating the distribution $P(\tau_D)$ from the autocorrelation function[2]

$$G(\tau) = \int P(\tau_D)\left(1 + \frac{\tau}{\tau_D}\right)^{-1}\left(1 + \left(\frac{w_{xy}}{w_z}\right)^2 \frac{\tau}{\tau_D}\right)^{-\frac{1}{2}} \mathrm{d}\tau_D \tag{6}$$

This challenge is also encountered in analysing dynamic light scattering (DLS) correlation functions. Different solutions have been developed to gain diffusion time distributions. It can be achieved by an Tikhonov regularization under constraint conditions using an inverse Laplace transform known as CONTIN[52–54] or by the method of histograms as described by Starchev *et al.*[38] A different strategy uses a maximum entropy method to provide a bias-free fitting of the data with a quasi-continuous distribution of a large number of diffusing components.[55]

Anomalous diffusion

An important issue for translational diffusion measurements is the question whether translational diffusion is normal or not. Deviations from normal diffusion can be caused by internal chain motions[11,13,56] of (bio-)polymers, by molecular crowding,[20,56–61] or the restriction of diffusion to a certain "corral" region.[62] Different approaches have been suggested to deal with anomalous diffusion. One of the possibilities to describe anomalous diffusion uses a power law scaling of time t^{α}.[13,57–59,63,64] The scaling parameter α can depend on the time scale investigated and thus allows for a distinction between translational and chain diffusion.[11] Another possibility consists in using a multicomponent fit as shown in eqn (5) assuming diffusion through a spatially heterogeneous medium with a certain number of different diffusion coefficients.[57,59]

Apart from the above mentioned analytical tools, a technical approach to detect anomalous diffusion has been reported. Sample-volume-controlled-(SVC-) FCS can directly detect anomalous diffusion by changing the diameter of the collimated excitation laser beam.[60,65,66] One of the challenges of this approach is however the control over the optical parameters such as distortions of the confocal volume.[67]

It should be emphasized at this point, that FCS correlation curves can be often fitted equally well by an anomalous diffusion model and using two diffusion time constants according to eqn (5). However, it has to be carefully analysed which of the two models is more appropriate. Combining FCS results with simulations,[68] Vagias *et al.* for example showed that for the case of attractive tracer-polymer interactions, only a two-component diffusion process (eqn (5)) is a physically meaningful model.[69]

Rotational diffusion

In addition to translational diffusion, rotational diffusion of fluorescent probes can be observed for anisotropically emitting

probes with a fixed dipole moment such as single molecules[70–73] or semiconductor nanorods.[74] The theory to analyse rotational diffusion from FCS measurements was developed by Ehrenberg/Rigler[75] and Aragon/Pecora.[76,77] The drop in correlation due to rotational motion appears around the rotational diffusion time τ_R which is typically found in the ns to μs range, *i.e.* on much shorter timescales compared to τ_D of translational motion. One technical problem for measuring correlations on such short time scales is that measurements with one APD possess a dead time in the same temporal range and thus cannot detect two photon arriving events that are temporarily closer than that period. In order to obtain correlation values at times shorter than this dead time, a Hanbury Brown and Twiss setup[78] should be used which splits the emission light and detects the photons on two independent detectors.[79,80] Cross-correlation of the photon arrival times on the two detectors enables full correlation fluorescence correlation spectroscopy (fcFCS) measurements from the time range of picoseconds to the several minutes (see Fig. 3).

Technical and methodical developments

Several technical and methodical developments of FCS have been reported which broaden the range and accuracy of FCS measurements.

One important step was the introduction of dual-focus FCS (2fFCS) by Enderlein and co-workers.[81] In 2fFCS measurements, the laser focus is switched between two positions. The distance between both laser foci serves as an internal distance reference, *i.e.* an intrinsic ruler. Thus reference measurements for relating diffusion time and diffusion coefficient become unnecessary. The accuracy of the obtained diffusion coefficients even allows for a sensitive measurement of temperature on a micrometre scale.[82] 2fFCS bears the huge advantage that, due to its robustness against optical and photophysical artefacts, it allows for the investigation of systems with inherently large optical aberrations as they may occur in a variety of polymer systems.[83] In particular, in single focus FCS, slight changes in the refractive index,[84] coverslip thickness, laser beam geometry or optical saturation can cause severe distortions of the confocal volume[67,85] and, thus, can result in significant errors and misinterpretations, especially in cases requiring accurate diffusion measurements. These problems are significantly reduced in 2fFCS. Another benefit from 2fFCS is that it greatly reduces the dependency of FCS results on the size and shape of the excitation volume which due to optical saturation effects can vary significantly with excitation intensity. However, when rather large colloids or macromolecules are used as probes for 2fFCS, their size with respect to the excitation laser focus has to be taken into account.[86]

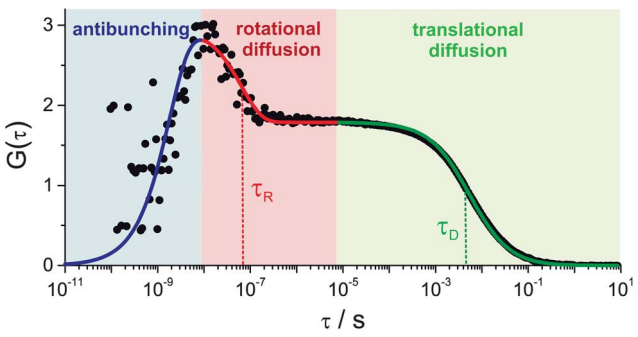

Fig. 3 Full correlation FCS cross-correlation function for a perylene diimide derivative measured at 80% conversion of a free radical bulk polymerization of styrene showing the drops in the correlation curve due to rotational and translational diffusion and the rise in the nanosecond range due to antibunching. The latter is caused by the fact that a single molecule, after emission of a photon, statistically requires some time to be re-excited and emit another photon. (Adapted from Dorfschmid *et al.*[71])

Limiting the excitation volume allows for a higher spatial resolution of FCS measurements or selective spatial restriction *e.g.* to interfaces. Dynamic processes at liquid–solid interfaces can be studied using total internal reflection FCS (TIR-FCS).[87–91] This technique exploits the possibility to restrict the axial dimension of the excitation volume to a depth of *ca.* 100 nm using the evanescent wave of a laser beam totally reflected at the solid–liquid interface. It allowed Koynov and co-workers to measure single molecule and quantum dot diffusion coefficients at water–glass interfaces.[88] Another way to gain spatial resolution beyond the diffraction limit of light is the combination of FCS and stimulated-emission-depletion (STED) nanoscopy,[92,93] where the excitation volume is minimized by an intensive donut-shaped STED laser pulse which depopulates basically all excited states except for a central volume of sub-diffraction size.

Further powerful technical developments are FCS with two-photon excitation,[40,94–97] spatial fluorescence cross correlation spectroscopy (FCCS) which can be used to investigate microflows,[98] dual-colour FCCS to correlate the fluctuations from two spectrally distinct fluorophores in order to analyse kinetics or association,[15] pulsed interleaved excitation (PIE) FCS,[73,99] fluorescence triple correlation spectroscopy (F3CS),[100] filtered FCS[101] and multiparameter FCS[102] to gain the maximum amount of information from a single FCS experiment.

One technical development that should additionally be emphasized for FCS measurements in polymer systems is the extension of the available temperature range. Compared to biological systems, a much broader range from cryogenic temperatures up to several hundred degrees centigrade is required to capture all the interesting transitions in polymers. Fluorescence microscopy studies in the elevated temperature range above *ca.* 80 °C have been reported,[103–105] and will extend the breadth of FCS studies in polymer systems.

Limitations and pitfalls for FCS measurements in polymers

Despite their high versatility, FCS measurements also possess some intrinsic limitations and pitfalls which should always be kept in mind.

In particular, slight changes in the refractive index, coverslip thickness, laser beam geometry, pinhole adjustment or optical saturation can cause severe distortions of the confocal volume[67,85,106] and thus can result in significant errors and misinterpretations, especially in heterogeneous systems or at interfaces with significant refractive index change. The effect of

refractive index mismatch for different confocal microscopes has been described.[107] Depending on the polymer and solvent, it can cause severe problems in polymer systems, the refractive index of which can differ significantly from the value in water. Thus, the confocal volume can be significantly distorted, and in this case calibration of the diffusion time with the typical reference dyes such as Rh6G in water results in errors.[108] Therefore, alternative calibration methods had to be found. Zettl *et al.* used the known molecular weight dependence of the diffusion of rhodamine B (RhB) labelled polymer chains of different lengths in very dilute solution to determine the size of the confocal volume and thus to calibrate the diffusion coefficient obtained by FCS.[109,110] The observation volume can be also calibrated using fluorescently labelled silica nanoparticles[111,112] or dye-labelled polystyrene (PS) of known molecular mass,[113] with the diffusion coefficient in dilute solution known from DLS measurements. One convenient workaround to reduce the errors concerning distortions of the confocal volume is to measure at relatively small penetration depths of *ca.* 10 μm which is still reasonably far in the solution to avoid biased results due to influences of the interface.

Another critical aspect is the spatial resolution of FCS which has been recently discussed in some papers.[47,48] For certain cases, FCS is capable of resolving dynamics at the nanoscale, *i.e.* far beyond the limits of optical resolution.[48] In general, however, the limits of its spatial accuracy have to be considered.[47] Thus, for systems with heterogeneities on the nanometre scale, one has to be aware that the obtained diffusion coefficient averages over these heterogeneities. The same is true for temporal heterogeneities such as mesh size fluctuations or fast structural changes. Even though photon arrival times can be determined with picosecond accuracy, the correlation analysis performed after the FCS measurements averages over the measurement time. Therefore dynamics within such short times remains obscured, unless an appropriate model is explicitly implemented into the autocorrelation fit function. Furthermore, in order to obtain reliable diffusion coefficients for complex systems, it has been reported that the minimum lag time, the maximum lag time and the averaging time are critical parameters which have to be chosen appropriately.[114]

Apart from diffusional processes, decays in the autocorrelations curves can also occur as a result of photophysical and photochemical processes. In particular, the contribution of saturation effects and triplet blinking have been investigated[115,116] and the rates of intersystem crossing and triplet decay as well as the excitation cross section of fluorophores could be determined.[117] Therefore, the choice of appropriate dyes is essential to obtain meaningful results. However, a good dye should not only show suitable photophysics, but also serve as a selective label to observe the diffusing species of interest.

Diffusion of polymer chains in pure solvents

Depending on the interactions with the solvent, polymer chains possess different conformations with different sizes which can be elucidated using FCS. According to the Stokes–Einstein equation

$$D = \frac{kT}{6\pi\eta r_h} \quad (7)$$

the hydrodynamic radius r_h of the diffusing species can be determined from the measured diffusion coefficient D and the known viscosity η of the solvent.

Using this approach in combination with diffusion-ordered NMR experiments, effects of size, functionality, and peptide secondary structure on the diffusion coefficient and hydrodynamic radius of poly-Z-L-lysine functionalized polyphenylene cores were investigated.[111] Furthermore, for π-conjugated polymer solutions in toluene, Murthy *et al.* found a larger diffusion coefficient for high molecular weight polymer chains (*ca.* 300 kDa) compared to low ones (*ca.* 50 kDa).[118] This unexpected result was explained by the compact globular conformation of the high molecular weight chains in contrast to the voluminous aggregates formed by the shorter polymer chains.

Using the typical FCS analysis to determine the diffusion of very long polymer chains can result in significant errors if the polymer size approaches the size of the confocal volume or even exceeds it. A model only considering the centre of mass diffusion becomes inappropriate since also changes in chain conformation, *i.e.* chain diffusion, contribute to the correlation curve. For this case, Winkler determined an analytical expression for the FCS correlation function including translational and rotational motion for rod-like polymers on the basis of a Gaussian semiflexible chain model.[119]

Diffusion in polymer solutions, gels, melts and glasses

FCS is uniquely suited to explore polymer dynamics in solution. For this purpose, a small amount of fluorescently labelled polymer chains or free dyes is added to the polymer solutions or *vice versa*. One very interesting aspect of polymer solutions is the concentration and molecular weight dependence of the diffusion of dye-labelled polymer chains and molecular probes. Principally, three different polymer concentration regimes can be distinguished: (i) dilute solutions in which diffusion is fully governed by the hydrodynamic radius of the diffusing species, (ii) semidilute solutions in which the polymer coils start to overlap, (iii) concentrated solutions in which the chains strongly interact with each other. The semidilute and the concentrated solutions can be further divided into an unentangled and an entangled regime. In the latter, topological constraints caused by entanglement dominate the dynamics. The transition between the regimes depends primarily on concentration and molecular weight of the polymer, as shown in Fig. 4. At even higher polymer concentration, a transition to the glassy state appears and polymer dynamics is controlled by the available free volume. Depending on the intermolecular interactions of polymer chains, their (partial) crystallization is also a process which should be taken into account.

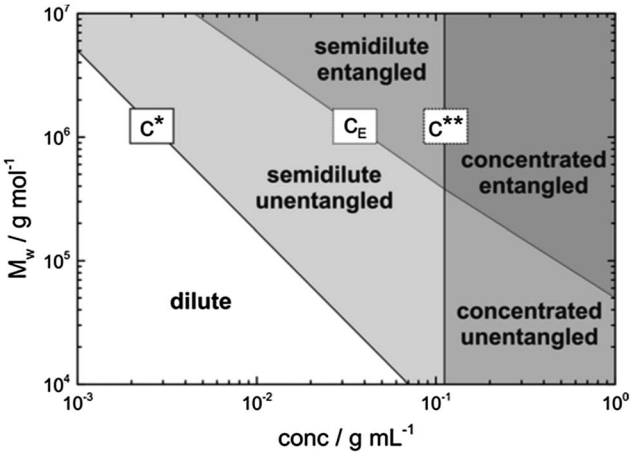

Fig. 4 Regimes of polymer solutions in terms of concentration and molecular weight for a polymer in a good solvent, *e.g.* polystyrene in toluene. (Adapted from Graessley and Magda *et al.*[120,121])

In the following, the contributions of FCS to elucidate molecular dynamics in the various regimes will be discussed.

Diffusion of small molecular probes and nanoparticles in polymer solutions and melts

The diffusion of single molecules and nanoparticles provides important information about the local mechanical and viscoelastic properties of the polymer solutions, *i.e.* their nanorheology. In contrast to the macroviscosity "felt" by large objects, the nanoviscosity refers to the diffusion or the drag of small objects such as molecules or small nanoparticles. Hence, viscosity is a strong function of the length scale at which it is probed.[122,123] The obvious question which arises from this relation concerns the length scale at which nanoviscosity switches to macroviscosity.

Holyst *et al.*[124] addressed this issue by studying the diffusion of differently sized probes ranging from RhB molecules (1.7 nm) up to silica spheres (114 nm) in polyethylene glycol (PEG) solutions with a combination of FCS, capillary electrophoresis and macroviscosity measurements (see Fig. 5). They found that the large probes diffused as expected from the macroviscosity of the solutions whereas the diffusion of the small probes was clearly faster. They seemed to experience an up to 100× smaller nanoviscosity. Such a behaviour was also observed by Michelman-Ribeiro *et al.*[125] for the diffusion of 2 to 44 nm sized probes in PVA solutions. The crossover from probing nanoviscosity to probing macroviscosity was found at a length scale at which the probe reached a size of approximately the radius of gyration of the polyethylene glycol (PEG) polymer under investigation.[124] It could be shown that the dependency of viscosity η on the ratio between an effective probe size and the correlation length ξ of the polymer follows a stretched exponential function. Probes smaller than the radius of gyration R_g of the polymer, experience the nanoviscosity and the effective probe size is the probe radius R, whereas it equals the radius of gyration R_g for probe molecules of larger size which feel the macroviscosity of the polymer solution.[124] Thus,

$$\frac{\eta}{\eta_0} = \begin{cases} \dfrac{\eta_{\text{nano}}}{\eta_0} = \exp\left(b\left(\dfrac{R}{\xi}\right)^a\right) & \text{for } R < R_g \\ \dfrac{\eta_{\text{macro}}}{\eta_0} = \exp\left(b\left(\dfrac{R_g}{\xi}\right)^a\right) & \text{for } R > R_g \end{cases} \quad (8)$$

where the ratio between radius of gyration and correlation length ξ depends on the polymer concentration and the overlap concentration according to

$$\frac{R_g}{\xi} = \left(\frac{c}{c^*}\right)^{0.75} \quad (9)$$

Using the relationship shown in eqn (8), all measured data of viscosity *versus* probe size could be plotted on one master curve.

From the above considerations it becomes also clear that an estimation of the translational diffusion coefficient from the Stokes–Einstein (SE) relation using the known polymer macroscopic viscosity is only reliable for probes larger than R_g and fails for small diffusants.[124,126]

Since the dependency of viscosity on polymer concentration shows a stretched exponential behaviour, this is also expected for the diffusion coefficient, *i.e.*

$$D = \frac{kT}{6\pi R\eta} = D_0 \exp\left(-b\left(\frac{R}{\xi}\right)^a\right) \quad (10)$$

Such stretched exponential functions were observed in several FCS studies. They were put forward by Phillies[127] and could be used for many observables in polymer solution such as self-diffusion, viscosity, rotational diffusion, electrophoretic mobility, dielectric relaxation and sedimentation. However, it should be kept in mind that there are also different approaches for scaling laws such as the free-volume theory of Fujita,[128] its more complex extension by Vrentas and Duda,[129] and the scaling model of Petit *et al.*[130] All of these models gave a reasonable fit *e.g.* for the diffusion of small dye molecules in octane swollen linear PDMS at different degrees of swelling.[131]

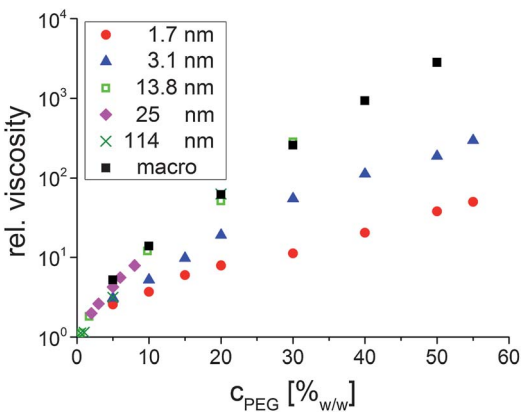

Fig. 5 Viscosity determined using diffusion measurements of differently sized probes in PEG 20 000 solution. Small probes experience nanoviscosity whereas large probes follow the macroviscosity. The crossover length scale between nano- and macroviscosity in PEG 20 000 is larger than 3.1 nm and smaller than 13 nm. (Adapted from Holyst *et al.*[124])

The diffusion coefficients of a perylene monoimide dye for various concentrations of solutions of different molecular weight polystyrenes in acetophenone all fall onto the same master curve which could be fitted with a stretched exponential.[132] From the perspective of the probes, the change in molecular weight of the polymer between 110 and 450 kg mol^{-1} does not seem to make a difference. Additionally, at low polymer concentrations, the diffusion of the small probes is also not significantly influenced by the presence of polymer chains since it can diffuse basically unhindered through the polymer meshes. In another study, stretched exponential behaviour was found for the diffusion coefficient of 2.5 nm gold nanoparticles in solutions of PS (R_g = 18 nm) in toluene using fluctuation correlation spectroscopy. In contrast to FCS, the luminescence of gold nanoparticles excited with multiphoton absorption was observed.[126] In these studies a concentration range between ~6c* and 20c* was investigated. At high polymer concentrations, the authors found a subdiffusive behaviour of the nanoparticles, whereas a small molecular probe (coumarin 480 measured using FCS) exhibited normal diffusion behaviour. Thus, the size of the probes with respect to the mesh size determines whether the diffusion is normal or anomalous.

In polymer melts of various molecular weights, the diffusion of molecular tracers was found to sense local segmental dynamics depending on the glass transition temperature of the polymer matrix, but not on its macroscopic viscosity.[133,134] The temperature dependence of the diffusion coefficient followed a Vogel–Fulcher–Tammann function with an activation energy increasing with the tracer size and depending on the polymer. In a PS/poly(methyl phenyl siloxane) blend, two polymer components with a difference in glass transition temperature of more than 113 K and an upper critical solution temperature, a combination of FCS and laser scanning confocal microscopy allowed for monitoring the dynamics of phase separation.[135] It was also shown, that in polymer blends, the topology of the matrix polymer plays a pivotal role. A comparison between the diffusion of terrylene diimide probes in the polymer melt of linear and star-shaped 1,4-polyisoprenes gave different results.[57] For the experiment with linear polymer chains, the autocorrelation curves could be fitted with one diffusion time, thus indicating a system homogeneous on the length scale of FCS, whereas the autocorrelation curves of the probe molecules in the solutions of star polymers could be best described by assuming two time constants. It was assumed that the fast time constant corresponds to a tracer diffusion comparable to that in the linear polymer. The slow time constant was related to topological restrictions causing retention of the tracer. Therefore, FCS allows for the detection of heterogeneity on the nano- to micrometer length scale. This makes FCS a very powerful technique to analyze polymer networks and crosslinking polymerization as described below.

Diffusion of small molecular probes and nanoparticles in covalently crosslinked polymer gels

In this section, I will concentrate on diffusion measurements in gels with permanent, covalent crosslinks. This situation has to be distinguished from (non-covalent) chain interactions due to entanglements in concentrated polymer solutions.[131] Diffusion in gels is a complex phenomenon affected by several factors, such as the mesh size of the gel, its microstructure, the degree of swelling, the size of the diffusing species, and interactions between diffusing species and gel.

Michelman-Ribeiro reported on the diffusion of 5-carboxytetramethylrhodamine (TAMRA) in poly(vinyl alcohol) (PVA) solutions and gels prepared at various polymer concentrations and crosslink densities.[136] As shown in Fig. 6, they found that below a certain threshold PVA concentration (in their case approx. 3% w/v), the diffusion of the probe was independent of the crosslinking density. At higher concentrations, the diffusion of stronger crosslinked gels decreased more rapidly when increasing the polymer concentration, as also confirmed in other studies.[131,137] The authors found a simple linear relation between the difference of diffusion times [τ(gel) − τ(solution)] of the probe in the gel and the non-crosslinked polymer solution and the elastic modulus of the same gel, indicating that diffusion of the probe particles is strongly correlated with the gel elasticity.

FCS studies on the diffusion in highly swellable synthetic crosslinked PEG hydrogel matrices demonstrated the feasibility of free volume theory to describe the dependency of solute diffusivities on the solute size and the swelling ratio of the gels.[138] The probes used for these studies were Rh6G and three proteins with hydrodynamic radii between 1 and 5 nm, and therefore significantly smaller than the mesh size of the polymer gels of *ca.* 14–19 nm.

Modesti *et al.* used FCS to study the diffusion of hydrophobic dye molecules in octane-swollen poly(dimethyl siloxane) linear-

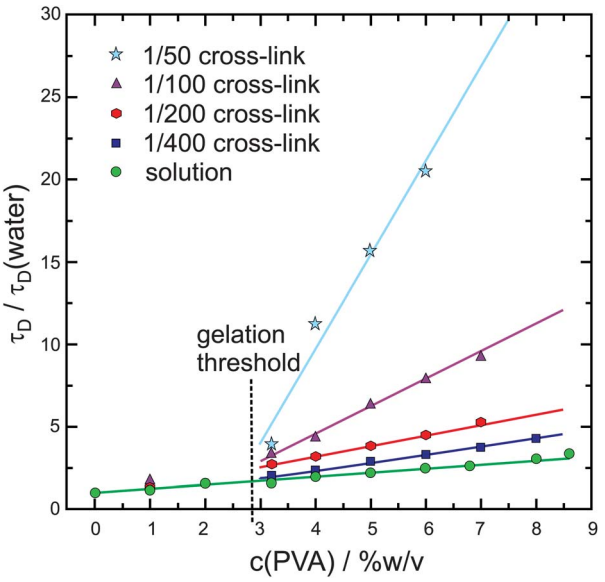

Fig. 6 Scaled characteristic diffusion time of fluorescent TAMRA molecules in PVA solutions and gels at several crosslink densities as a function of polymer concentration with linear fits. The times are scaled by the diffusion time of the probe in water. The vertical dashed line indicates the approximate gelation threshold. (Adapted from Michelman-Ribeiro *et al.*[136])

chain solutions and end-linked model networks, which were at an equilibrium degree of swelling, and compared the results with pulsed-field-gradient nuclear magnetic resonance (PFG-NMR) data of octane diffusion.[131] The small octane molecule did not show crosslink-dependent behaviour whereas the larger dye became more restricted with increasing crosslink-density. The most reasonable description of their results was obtained by assuming that the crosslink effect is additive to the effective friction coefficient of the probes, *i.e.* the friction coefficient in the network equals the effective friction coefficient for the probe in the pure solvent plus a friction coefficient caused by the permanent crosslinks. Deviations from this picture, however, were found for very high crosslink density and were rationalised by more pronounced swelling heterogeneities, *i.e.* the solvent preferably swells the more weakly crosslinked matrix and thus, even at rather low degrees of swelling, opens up percolating regions of lower polymer density in which the dye can diffuse rather easily.

Apart from studies in readily synthesized polymer gels, FCS was used to address photo-crosslinking of PS microbeads using UV light.[139] The authors found that swelling of the core of the microbeads was the same with and without UV irradiation indicating that no photo crosslinking appeared in the core. Thus, they assumed that UV crosslinking effects are limited to the shell only, presumably due to inner filter effects.

FCS to follow polymerization processes

Diffusion plays an important role for polymerization processes. In particular during bulk polymerizations, rate constants can reach their diffusion limit already at the viscosities present at moderate conversions. We followed the diffusion of differently sized dyes during free radical bulk polymerizations using a combination of FCS and widefield fluorescence microscopy. It was found that the relative changes in diffusion coefficients scale differently depending on the size of the probing dye,[71] in disagreement with the Stokes–Einstein-equation (eqn (7)) where all diffusion coefficients normalized to their value in monomer solution should lie on a master curve. Interestingly, a master curve was obtained for the normalized rotational diffusion coefficients D_R as measured using fcFCS, indicating that the Stokes–Einstein–Debye equation

$$D_R = \frac{kT}{8\pi\eta {r_h}^3} \quad (11)$$

is valid for all sizes of the dyes used. We attribute this size-dependent behaviour of the translational and rotational diffusion of the probes to the fact that only a small free volume is needed for rotational motion of the dyes whereas to detect translational motion, they have to move a significant distance through the meshes of the polymer. It makes also a significant difference if the meshes are physically or chemically crosslinked. Addition of crosslinker to the polymerization system resulted in the appearance of two distinct diffusion coefficients at the gel point which were attributed to the appearance of microgel regions.[140] In microgel regions of higher polymer density,[141] the probes diffuse significantly slower than in the other regions of lower polymer density. With on-going polymerization, the fraction of probes in the denser regions continuously increased. Chemical crosslinking is not a necessary condition for the appearance of heterogeneity, *i.e.* different diffusion coefficients. They were also observed in the gel effect region during the linear polymerization of methyl methacrylate,[142] where this heterogeneity appears already at a rather low conversion of 20% and thus might attribute significantly to the strong Trommsdorff effect observed in this system.

Diffusion of macromolecular probes and larger-sized nanoparticles in polymer solutions and glasses

In the following, an overview of FCS studies on the diffusion of fluorescently labelled macromolecules in the polymer concentration regimes shown in Fig. 4 is given. Most studies were performed on labelled PS chains in toluene solutions of non-labelled PS of similar length. For highly dilute and non-interacting solutions, this allows for the determination of self-diffusion coefficients.

In the diluted regime, the diffusional dynamics is dominated by the hydrodynamic radius of the diffusing probe. The diffusion coefficient can be approximated by a linear dependence on polymer concentration[109] according to the Kirkwood–Riseman theory:[143]

$$D = D_0 - k_f \cdot c \quad (12)$$

where D_0 is the diffusion coefficient at infinite dilution and k_f is a proportionality factor. Both constants depend on the system under investigation. If both parameters are known, they can be used to determine the size of the confocal volume as described earlier in this review.

The transition between dilute and semi-dilute solutions is defined by the overlap concentration c^* which is described by[110,144]

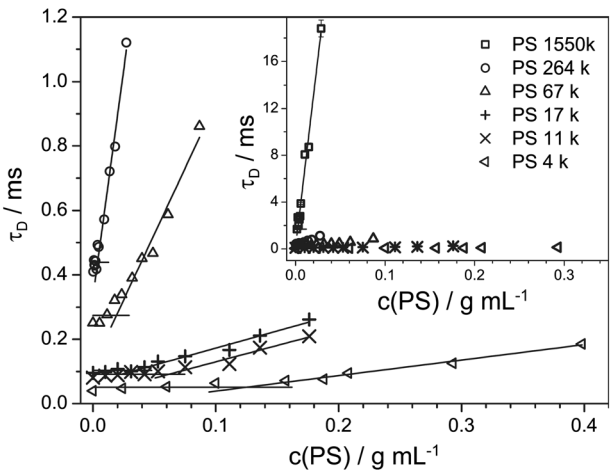

Fig. 7 Dependency of the probe diffusion time on the concentration of PS solutions in toluene for different molecular weights of the dissolved polymer. The inset shows a wider scaling on the vertical axis (adapted from Zettl *et al.*,[110] Copyright 2007 by The American Physical Society).

$$c^* = a^{-3}N^{1-3\nu} = \frac{1}{a^3 M^{1-3\nu}} M_w^{1-3\nu} \quad (13)$$

with the length a of a single polymer segment, the degree of polymerization N, the molecular weight M of a monomer unit, the weight average molecular weight M_w and the Flory exponent ν. FCS measurement have verified that the concept of an overlap concentration is very useful.[110] Fig. 7 shows plots of the diffusion times of PS chains of different molecular mass *versus* their concentration in toluene, a good solvent for PS. The diffusion times of the dilute and the low concentration part of the semidilute regime can be linearly fitted and the two fits intersect at the overlap concentration c^*. For increasing molecular mass, c^* shifts to lower concentrations. Its dependency on molecular mass could be fitted well with eqn (13) which resulted in a Flory exponent of 0.59 in excellent agreement with the value of 0.588 predicted by theory for a polymer in a good solvent.

Liu *et al.* investigated the motion of high molecular weight PS chains (M_w = 390 kg mol^{-1}) in toluene in a broad polymer concentration range between 10^{-4} and 0.4 g mL^{-1}.[113] In the dilute regime ($c < c^* \approx 0.01$ g mL^{-1}), they observed basically only minor changes in the diffusion coefficient with increasing concentration, *i.e.* $D \sim c^0$. In the unentangled semidilute regime ($c^* \approx 0.01$ g mL$^{-1} < c < c_E \approx 0.02$ g mL^{-1}) the polymer coils overlap but do not entangle effectively, resulting in a scaling of $D \sim c^{-1/2}$ in agreement with theory.[145] As soon as entanglements start to dominate the diffusional behaviour at $c > c_E \approx 0.02$ g mL^{-1}, the scaling changes to $D \sim c^{-7/4}$ as predicted by basic scaling and reptation theory.[144,146] In Fig. 8, a double-logarithmic plot of the diffusion coefficients obtained using FCS *versus* the polymer concentration is presented. The data could be well fitted with the above mentioned scalings for the different regimes. The transition between them, however, was found to be rather smooth. Very similar scaling laws were obtained for the diffusion of perylene–monoimide-labelled PS chains in unentangled and entangled semidilute solutions.[132] In semidilute solutions of low molecular weight, polymer chains that do not entangle, and the polymer-bound dye shows similar behaviour to free dyes sensing simply the increase in local viscosity with a temperature dependence as described by an Arrhenius behaviour.[95] The obtained activation energies of diffusion showed a significant increase with increasing polymer concentration and could be related to free volume theory.[147]

The diffusion of polymer chains is also molecular weight dependent. For PS in the good solvent toluene, a scaling of $D \sim M^{-3/5}$ and $D \sim M^{-2}$ for dilute and semidilute entangled solutions was determined, respectively.[56] Cherdhirankorn *et al.* investigated the diffusion of labelled PS chains in toluene solutions of polystyrenes of different molecular mass.[132] They found that higher molecular weights of the matrix polymer result in slower diffusion of the macromolecular probes as long as the molecular weight of the matrix does not exceed 5 times the molecular weight of the probe. In the latter case, a double-logarithmic plot of D normalized to the diffusion coefficient in infinite dilute solution *versus* the polymer concentration normalized to the overlap concentration of the diffusing fluorescent labelled polymer species resulted in a master curve, again with a slope of −0.5 in the unentangled semidilute and −1.75 in the entangled semidilute regime.

In addition to the self-diffusion coefficient of polymer chains, their collective diffusion and the interplay between these two types of diffusion is of considerable interest and was shown to have significant impact, for example, on the production of nanofibres.[56] Collective diffusion can be studied by dynamic light scattering, whereas for self-diffusion, PFG-NMR and label techniques such as forced Rayleigh scattering or FCS are applied. In a comparative study with DLS, Zettl *et al.* showed that FCS allows for measurements of collective diffusion and thus is a very powerful method to compare both types of diffusion within exactly the same systems.[56] In addition to self-diffusion, they found a collective diffusion mode in the FCS

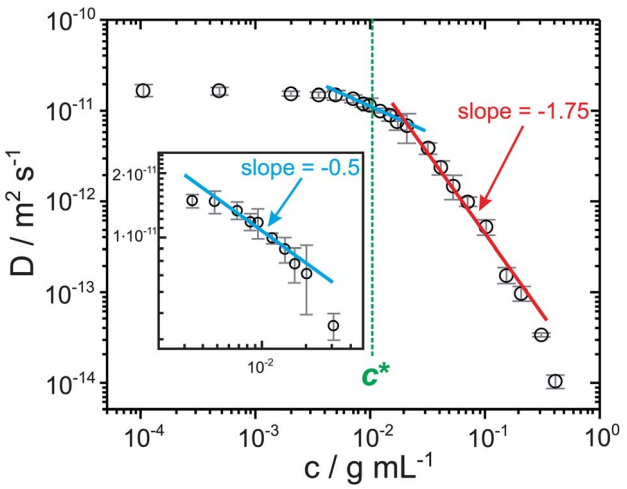

Fig. 8 Diffusion coefficient of labelled PS (M_w = 3.90 × 10^5 g mol^{-1}, M_w/M_n < 1.10) in toluene solutions as a function of polymer concentration and its prediction according to reptation and scaling theory. (Adapted with permission from Liu *et al.*[113] Copyright 2005 American Chemical Society.)

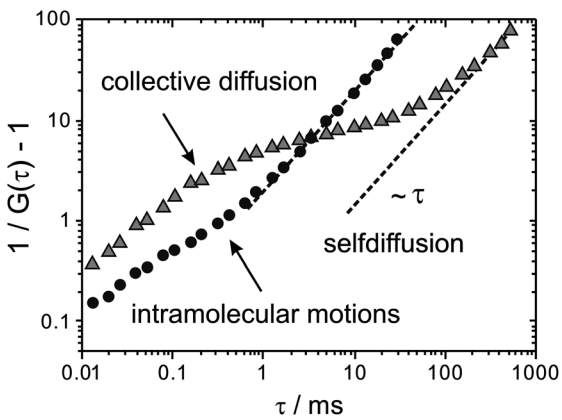

Fig. 9 The function $1/G(\tau) - 1$ of 515 kg mol^{-1} PS chains in dilute solution (circles, $c \rightarrow 0$) and in semidilute solution (triangles, c = 13 wt%). The dashed lines of slope τ characterize self-diffusion. Intramolecular motions and collective diffusion dominate in dilute and semidilute entangled solution, respectively, for short times. (Adapted from Zettl *et al.*[56])

autocorrelation curves in semidilute solutions which scales with $D_c \sim M_w^0\, c^{3/4}$ and depends on the molecular weight of the matrix polymer, but not on the molecular weight of the tracer itself.[148] In Fig. 9, a comparison between the FCS autocorrelation curves (presented as their reciprocal value minus 1) of a very dilute and a semidilute PS solution is presented.[56] At long times of $\tau > 1$ ms for dilute and $\tau > 200$ ms for semidilute solutions, an exponential dependence of the autocorrelation on time is obtained. At shorter times, deviations are obvious. In the case of dilute solutions, the slight change in slope in Fig. 9 can be related to intramolecular motions within single polymer chains. For semidilute solutions, rather large deviations appear which are caused by collective diffusion of polymer chains. The reason why such a collective mode can be observed by FCS, using only a small fraction of labelled polymer chains, lies in the long-range interaction of polymer chains through the network of transient entanglements. A very appealing visual explanation for this can be found in Zettl *et al.*[56]

Apart from the described diffusion studies on labelled PS chains, translational diffusion of Alexa-labelled polymethacrylic acid (PMAA) in aqueous solution was studied as a function of polymer concentration, solution pH, and ionic strength.[149] In agreement with the PS solution results, increasing the polymer concentration had little effect on the polymer diffusion up to the overlap concentration c^*. Beyond c^*, the diffusion coefficients dropped significantly with increasing polymer concentration. A change from pH 5 to pH 8 resulted in an increased charge on the PMAA chains resulting in their twofold expansion. Enhanced ion concentrations of alkaline metal ions caused a chain contraction. Both dependencies could be detected using FCS diffusion measurements.

Further FCS studies were used to study electrostatic interaction of charged polymers. In this way, the complexation between negatively charged rhodamine-labelled oligonucleotides and cationic polymers could be characterized.[150] Furthermore, the diffusion of cationic Rh6G dye molecules in anionic polystyrene sulfonate (PSS) polymers was investigated.[151] The autocorrelation curves had to be fitted with two diffusion times according to eqn (5) with $n = 2$, reflecting free probes and probes bound to the PSS-chains due to electrostatic interactions. The fraction of bound probes could be decreased by elevated salt levels indicating a dynamic exchange process between the free and bound cationic dyes. In another study, determination of the hydrodynamic radius of fluorescent labelled dextran could explain their solvent dependent uptake into polyelectrolyte multilayer microcapsules.[152]

For highly concentrated polymer solutions, there is only a limited number of techniques capable of following their slow dynamics. Also FCS reaches its limits when probe motion becomes so slow that the number of molecules moving into or out of the confocal volume within the measurement time is too small to allow for reliable statistics. Increasing the measurement time is often not straight-forward since all fluorescence dyes have only a limited photostability. If a dye bleaches within the confocal volume, it will fake a faster diffusional motion than its real value. To approach these systems, widefield fluorescence microscopy and subsequent single molecule tracking is a much better method and has been utilized to study the glass transition.[153]

Yet, FCS studies have been performed in concentrated solutions. Approaching the glass transition, subdiffusive motion was found as an additional mode on an intermediate time scale between the fast collective diffusion and the slow self-diffusion.[56] Casoli *et al.* performed FCS measurement in thin spin-coated PDMS film (of $T_g \sim -120$ °C) doped with a small amount of Rh6G molecules.[154] They concluded that due to electrostatic interactions, the dyes are arranged at the glass/polymer interface and intensity fluctuations reflected changes of molecular configuration of the dye which are caused by changes in the local mobility of the surrounding polymer matrix. Even though bulk viscosity was changed by two orders of magnitude, they only observed 4-fold changes in the FCS correlation time, indicating that FCS measurements probe the local viscosity which can differ significantly from macroviscosity.

Diffusion of large nanoparticles in polymers

The size of the probe plays a pivotal role for the analysis of polymer systems. As already discussed before, probe size with respect to characteristic length scales of the investigated system determines the dynamics to be measured. Using fluorescent spheres with diameters in the 100 nm range, allows for measuring spatially resolved viscosity on the length scale of micrometers. Hence this technique is often referred to as passive microrheology.[155–157] In addition to its spatial resolution, the big advantage of microrheology is that only tiny sample volumes are required, a challenge for other rheometers. Diffusion of nanoparticles with sizes between 1 and 140 nm in agarose gels have been analysed by Fatin-Rouge *et al.*[63] They estimated a critical hydrodynamic radius R_c for which trapped particles still displayed local mobility and defined a reduced size R_A/R_c of the diffusing particle with radius R_A. For R_A/R_c smaller than 0.4, slightly anomalous diffusion with a scaling parameter α of 0.93 was observed indicating that the diffusion of particles has to proceed through obstacles. For more strongly reduced sizes, the connectivity of the pores decreases rapidly, and the particles get trapped because percolating paths for them become very rare. This is the case in which they can be used for microrheology.

FCS studies in responsive hydrogels

Responsive hydrogels offer many possibilities for designing drug delivery systems, sensors, and synthetic tissue because they can adapt different structures depending on their environment, in particular temperature and solvent conditions. In order to exploit their potential, a detailed knowledge of their structure and dynamics at the nanoscopic and mesoscopic scale is necessary. So far, the most prominent responsive polymer is poly(*N*-isopropylacrylamide) (PNIPAM). Its most relevant feature is a lower critical solution temperature (LCST) at around 32 °C,[158] a temperature close to optimal physiological conditions. Below this temperature PNIPAM solutions in water are in

a swollen state. At the LCST a volume phase transition occurs and the gel collapses and expels water. A multi-faceted knowledge about diffusion within these responsive hydrogels under different conditions is essential for the above mentioned applications. Within the last years, several studies have shown the potential of FCS for studying diffusion in PNIPAM.

Diffusion of small molecules and labelled PNIPAM chains in PNIPAM hydrogels follows a stretched exponential dependency of the diffusion coefficient on polymer concentration, as already described above for other polymer solutions.[159] The PNIPAM chains can be crosslinked by hectorite clay particles. The gelation mechanism of such PNIPAM-clay nanocomposite hydrogels is of significant interest and has been approached using FCS.[160]

If the thermoresponsive PNIPAM gels are anchored to a solid substrate, their swelling behaviour is restricted to one dimension, an interesting system the FCS investigation of which is straight-forward.[137,159] Diffusion of Alexa 647 molecules and green fluorescent protein, respectively, both weakly interacting with this hydrogel, was studied for different crosslinking densities, solvent quality and temperatures. The two different probes were used to determine heterogeneities on the length scale of their sizes. At the large swelling ratios present at low temperatures, the diffusion of the small molecular tracer scales with the polymer volume fraction following a stretched exponential function, similar to the behaviour in non-attached gels, and can be described with one diffusion coefficient, indicating that the system is homogeneous on this nanolength scale. For the green fluorescent protein, with a cylindrical shape of a length of 4.2 nm and diameter of 2.4 nm,[161] deviation from this single Fickian diffusion can already be observed in this regime, suggesting the presence of heterogeneity. In the transition regime from the swollen to the collapsed state around the volume phase transition temperature, two fractions of molecules with different diffusion coefficients were found. One scales with the stretched exponential function as observed for lower temperature, the other is faster and represents the unhindered diffusion of molecules in the solvent. After the collapse transition occurred at a swelling ratio of about 1.5, all dye molecules were expelled from the collapsed hydrogel films.

This situation becomes even more complex for nanocomposites with a thermoresponsive PNIPAM component. Lehmann *et al.* investigated how temperature-sensitive swelling influences the coupling of PNIPAM microparticles to a surrounding macroscopic poly(acrylamide) hydrogel.[162] Using scanning 2fFCS, they could quantify the diffusion of labelled dextranes inside the microgel beads and in the surrounding hydrogel matrix. The formation of interpenetrating networks inside the embedded microgel beads depends on their crosslink density. If the beads are weakly crosslinked, these composite hydrogels form interpenetrating polymer networks. As a consequence, swelling and deswelling of the beads is obstructed and the mobility of embedded fluorescently labelled dextran probes is reduced. For highly crosslinked beads, the hydrogel matrix swells heterogeneously upon collapse of the embedded beads, indicating the formation of pores near their surface. Such behaviour allows for tailoring of pore structures, thus enabling a control of the motion through these systems.

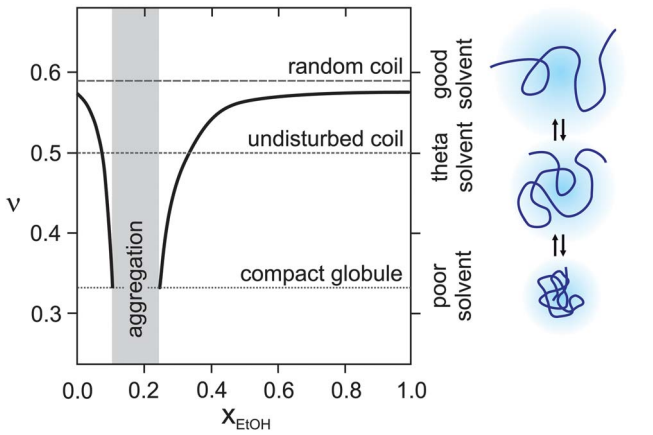

Fig. 10 Dependency of the Flory scaling parameter on the mol fraction x_{EtOH} of ethanol in water. The three dotted lines denote the theoretical values of the static scaling index for a random coil (0.588), an undisturbed coil (1/2), and a compact globule (1/3). On the right side a schematic drawing of the shape of polymer chains in the different regimes is presented. (Adapted from Wang *et al.*[166])

The layer-by-layer assembly of polyelectrolyte multilayers on PNIPAM microgels was evidenced using dual-color cross-correlation pulsed interleaved excitation FCS.[163] For this purpose, the first and the third cationic polymer were labelled with RhB and fluorescein isothiocyanate, respectively. After the layer-by-layer-absorption, the autocorrelation curves for both dyes and their cross-correlation show very similar diffusion times strongly suggesting that both labelled polyelectrolytes are attached to the same microgel. In addition, temperature-dependent FCS-measurements proved that the polyelectrolyte multilayer shell remains bound to the nanogel during the volume phase transition.[164]

Another not yet fully understood process in polymer science is cononsolvency,[165] *i.e.* the phenomenon that some responsive polymers are swollen in two different solvents, but not in certain mixtures of them. Wang *et al.* used FCS to study the cononsolvency in PNIPAM,[166] which is swollen in pure water or pure ethanol, but for a mixture of 80% water and 20% ethanol, exhibits a reduction in volume compared to the situation in the pure solvents. For their purposes they used fluorescently labelled PNIPAM of different degrees of polymerization and different water–ethanol compositions. They observed significant changes in the scaling of the hydrodynamic radius r_h (obtained from the diffusion coefficient, see eqn (7)) of PNIPAM. According to the mean-field approximation[167] and the scaling concept of polymers,[144] the hydrodynamic radius scales as $r_h \propto N^{\nu}$ with the degree of polymerization N and the Flory scaling exponent ν which depends on solvent conditions. The values in pure ethanol and pure water are close to the predicted values for athermal solvents, *i.e.* PNIPAM chains are random coils under these conditions. In water ethanol mixtures, the solvent quality for PNIPAM becomes significantly lower, reaching a limit of 0.33 when the mole fraction x_{EtOH} equals 0.09 and 0.25. Between these values, no uniform fluorescent signal could be detected in solution due to the (reversible) formation of suspended

aggregates. In summary, as shown in Fig. 10, the conformations of PNIPAM at different solvent mixtures could be elucidated using FCS.

The aspects concerning diffusion in PNIPAM brushes and micelle formation of thermoresponsive polymers, respectively, will be discussed in the following two sections.

Diffusion at solid–liquid interfaces

Diffusion of polymer chains at interfaces is rather complex and measurements as well as theoretical considerations are challenging. Several FCS studies were conducted at solid–liquid interfaces.

The Granick group studied the diffusion of end-labelled polyethylene glycol (PEG) chains adsorbed onto a hydrophobic self-assembled monolayer of octadecyltriethoxysilane coated onto a fused silica coverslip after two-photon excitation.[96,168] In this system, the polymer chains adsorb to the surface, thus exhibiting a flat 'pancake' conformation. Using PEG of different molecular weights (between 2 and 31 kg mol^{-1}), it was found that the diffusion coefficient scales with the number of chain segments according to a strikingly strong power-law scaling with an exponent of $-3/2$. Furthermore, it was investigated how surface diffusion is influenced by surface coverage.[169,170] At low surface coverages, an increase of the translational diffusion coefficient with increasing surface concentration was observed and attributed to a decrease of adsorption sites per molecule as chains switch from pancake to loop-train-tail conformation. At surface concentrations larger than the overlap concentration, the diffusion slowed down by one order of magnitude, due to crowding and entanglement with neighbouring chains.

Two studies dealt with translational diffusion within pH sensitive polymer brushes. Pan *et al.* investigated the diffusion in poly(acrylic acid) (PAA) chains grafted on PET surfaces.[171] The comparison of diffusion coefficients of labelled polymers and a free fluorescent probe allowed them to separate the effects of viscosity and relative molecular mass of the polymer. The dependency of diffusion on pH and ionic strength were analysed. Both factors influence the degree of swelling of the PAA layer. The diffusion of single positively charged Rh6G molecules in negatively charged supported sodium poly(styrene sulfonate) brushes at different pH values was investigated by Reznik *et al.*[172] They combined diffusion measurements using FCS with anisotropy measurements to analyse the rotational motion. Based on their results they suggest dynamic association of Rh6G molecules with the polymer brush, resulting in low energy nonspecific binding. Changing the pH can result in effective switching of ion transport rates since it affects the association and dissociation kinetics to the polymer.

Apart from pH, when a thermoresponsive polymer is used for coating, surfaces can be also sensitive to temperature. Wang *et al.* studied lateral diffusion of fluorescently labelled polyelectrolyte poly(2-vinylpyridine) (P2VP) on the surface of thermoresponsive poly(*N*-isopropylacrylamide) (PNIPAM) brushes.[112] At the low pH used for the measurements, the P2VP chains were fully charged and thus exhibited an extended coil conformation. Gradually increasing the temperature resulted in an increase in the diffusion coefficient of the P2VP probes as expected from the concomitant decrease of viscosity. However, at the volume phase transition temperature the diffusion coefficient started to decrease again. This behaviour was attributed to the collapse of the PNIPAM chain conformation changing the hairy to a closely packed layer.

Even though the above mentioned studies were conducted with normal FCS settings, it should be kept in mind that TIR-FCS which has been described in the section "technical developments" can increase the sensitivity of FCS measurements at solid–liquid interfaces.[88,89]

Studying micellization and aggregation

In analogy with studies on the dynamic properties of phospholipids[173] or low molecular weight amphiphiles,[174] micellization and aggregation of polymers can be also studied using FCS. In a first study, Nörenberg *et al.* investigated the formation of mixed polymer–surfactant micelles.[175] Most FCS studies, however, were performed on the micellization and aggregation behaviour of amphiphilic block copolymers which is expected to differ from common surfactants as the solvophobic and solvophilic parts of the molecule are much larger. Variation of the polymer concentration, quality of the solvent and the lengths of both blocks, results in a manifold of possibilities of forming different architectures such as spheres, disks, rods, vesicles, or flocs.[176]

Compared to other methods, FCS is especially powerful to detect a very low critical micelle concentration[174,176–179] (CMC) and a very low critical aggregation concentration[176–178] (CAC) as they often appear in block copolymers solutions. The sensitivity of FCS surpasses other fluorescence spectroscopy methods such as evaluating the ratio between two absorption bands of pyrene to detect the local polarity of its surrounding and, thus, the appearance of incorporation into micelles. The latter method only yields an upper estimate of the CMC.[179]

For concentrations below the CMC, the FCS curves can be fitted with one correlation time reflecting the presence of free fluorescence probes in solution. As soon as micelles or aggregates start to form and implement the probes into their structures, their motion becomes significantly slower and at least two correlation times, one reflecting the free probes and the other one related to the probes bound to micelles/aggregates, have to be used for fitting the autocorrelation curves. It could be nicely demonstrated by Bonné *et al.* that two correlation times appeared at the CMC and how the fraction of the slowly moving probe gradually increased with increasing polymer concentration, whereas the two correlation times remained constant[178] (see Fig. 11 and text below).

Apart from the determination of the CMC, the average size of micelles and aggregates[176–179] can be studied using FCS. The obtained correlation time can be used to calculate the translational diffusion coefficient of the fluorescent probe attached to the micelle using a reference of known diffusion coefficient. As already mentioned above, a common and reliable reference is Rh6G in water with a diffusion coefficient of 4.14×10^{-10} m^2 s^{-1}.[46] From the diffusion coefficient, the

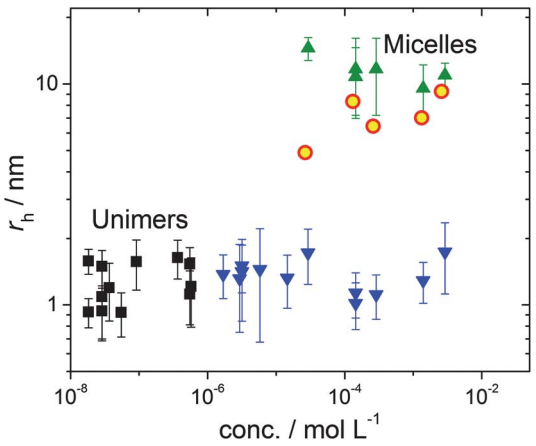

Fig. 11 (Apparent) hydrodynamic radii r_h as determined by FCS on P[(NOx)$_{10}$(MOx)$_{32}$] with different tracers. *Squares*: solutions containing only labelled copolymers; *triangles*: solutions containing both fluorescence-labelled and non-labelled copolymers; *circles*: solutions containing non-labelled polymers and Rh6G (adapted from Bonné *et al.*[178])

hydrodynamic radius of the micelles/aggregates can be determined using the Stokes–Einstein-equation (see eqn (7)). The determination of the micelle/aggregate size, however, can be strongly biased by the behaviour of the fluorescent probe, if the probe does not bind sufficiently to the micelles/aggregates. This has to be taken into account, in particular when free fluorescent probes are used which can reversibly bind to the micelles/aggregates. In many cases, it has been observed that the correlation time related to the micelles/aggregates becomes longer with increasing monomer concentrations and does not reach a constant value up to concentrations far above CMC (for some copolymers up to two decades). Only at higher concentrations a plateau value was obtained.[174,176] Thus, the apparent diffusion coefficient of the micelles seems to decrease and the hydrodynamic radius to increase, *i.e.* micelles seem to grow with increasing monomer concentrations. Such a dependence may be interpreted by the fact that the micellization of amphiphilic block copolymers with a liquid-like hydrophobic block is kinetically controlled rather than thermodynamically.[179]

A comparison with dynamic light scattering and with experiments of covalently fluorescence-labelled copolymers, however, did not reveal such an increase in hydrodynamic micelle radii.[178] The apparent increase of the radius was rather explained by the attachment of dyes to the micelles/aggregates. Binding of free dyes to micelles/aggregates is an equilibrium process and even though the chosen dyes are poorly water-soluble, and thus will be bound most of the time to the micelle/aggregate, there are also periods of free diffusion. These periods become shorter for higher micelle concentrations. Thus, even though the size of the micelles stays constant, the average time it takes a fluorescent probe to diffuse through the confocal volume becomes longer and the (time-averaged) diffusion coefficient smaller. Thus, the hydrodynamic radius seems to grow with increasing polymer concentration, and the magnitude of this effect will depend on the equilibrium constant of binding of the dye to the micelle. As a consequence, despite the fact that the addition of a small amount of a low molar mass dye to the polymer solutions is a straight-forward way of studying the aggregation of amphiphilic copolymers by FCS, great care has to be taken that the dyes show significant binding to the micelles. Otherwise, a wrong dependence of the hydrodynamic radii on polymer concentration will be observed, *i.e.* a too small radius will be obtained at low polymer concentration.

A less simple, but on the other hand more reliable alternative to circumvent these problems is to use probes covalently attached to the copolymers. A comparison between free and polymer-bound probes was performed by Bonné *et al.*[178] Fig. 11 shows this comparison between the FCS results in polyoxazoline block copolymers in aqueous solution. From the CMC up to high polymer concentrations, the hydrodynamic radii of the micelles obtained using partially labelled copolymers are constant and equal to the ones of labelled unimers measured at low concentrations. In contrast, the radius calculated using free Rh6G as a probe show a gradual increase from the CMC at approx. 10^{-5} M until 10^{-3} M before they reach the same value obtained with the covalently labelled system.

As already mentioned, a suitable system to study micelle formation with a free probe should have a high binding constant to the micelle. Furthermore, it is favourable if the non-bound dye shows lower or ideally no fluorescence compared to the micelle-bound dye. Octadecyl rhodamine B (ORB) has been reported as a system fulfilling both of the above mentioned properties. Therefore it is very suitable to probe the micellization of PS-poly(methyl acrylate) (PMA) block-copolymers.[180] The amphiphilic ORB binds strongly to the core–shell interface of the PS-PMA micelles with its nonpolar aliphatic tail buried in, and partially adsorbed to the PS core. Furthermore, the fluorescence from the water-dissolved dyes is self-quenched and does not significantly contribute to the monitored FCS fluctuations. In this PS-PMA-system, Humpolíčková *et al.*[180] also investigated the effect of different ORB concentrations. If the concentration of the fluorescent probe is lower than the concentration of the micelles, individual ORB molecules bind to different micelles and will not be self-quenched. The observed fluorescence of these probes is however lower than expected. The decreased intensity was attributed to hydrophobic impurities which are present in the micelle and quench the fluorescence. For a given amphiphile concentration the number of fluorescent micelles in the focal volume increases with increasing fluorescent probe concentration until it reaches a saturation limit. At this limit, each micelle is labelled. Further increase of the dye concentration results in a higher number of dye molecules per particle which increases the amplitude of fluctuations caused by the appearance and disappearance of multiple-tagged micelles. The autocorrelation function and the particle number, however, are not affected.

Several studies on micellization and aggregation using FCS were performed with polyoxazolines which are an interesting class of polymers since they are biocompatible and non-toxic, and immuno-response has not been reported.[181] The advantage

of this polymer class is that the polarity of each monomer unit can be fine-tuned by a suitable choice of the pendant 2-substituent. 2-Methyl- and 2-ethyl-2-oxazolines are hydrophilic, whereas side groups longer than propyl result in significant hydrophobicity. Thus, poly(2-alkyl-2-oxazoline) offers a manifold of possibilities to tune micellization and aggregation and thus allow for an adjustment of the properties related with these parameters. They also exhibit a volume phase transition with a lower critical solution temperature (LCST), comparable to PNIPAM, and their phase transition temperature can be easily tuned. Increasing the amount of hydrophilic 2-oxazoline monomer units increases the lower critical solution temperature (LCST), whereas hydrophobic units decrease the LCST. The polyoxazolines were covalently labelled with a tetramethylrhodamine isothiocyanate fluorophore and their micellization behaviour studied.[177] The position of the label, *i.e.* whether it was attached to the end of the hydrophobic poly(2-*n*-nonyl-2-oxazoline) block or the hydrophilic poly(2-methyl-2-oxazoline) block, was shown to have no influence on the FCS results on micellization.[178]

Apart from studying micellization of polyoxazolines, their thermo-responsive aggregation behaviour around the cloud point was investigated using FCS with varying temperature from r.t. up to *ca.* 50 °C.[182] For this purpose, different combinations of iso-propyl- (^{i}PrOx) and *n*-propyl- (^{n}PrOx) and *n*-nonyl- (NOx) substituted polyoxazolines were synthesized. From a combination with turbidimetry and small-angle neutron scattering measurements, the model shown in Fig. 12 and explained in the following was derived. The thermoresponsive P(^{i}PrOx) and P(^{n}PrOx) homopolymers exhibit a behaviour similar to the one encountered with other thermo-responsive homopolymers, such as PNIPAM.[183] For both homopolymers, the cloud point depends significantly on concentration and on the degree of polymerization. With increasing concentration and increasing degree of polymerization, the cloud point decreases. Both homopolymers were dissolved as unimers at room temperature.

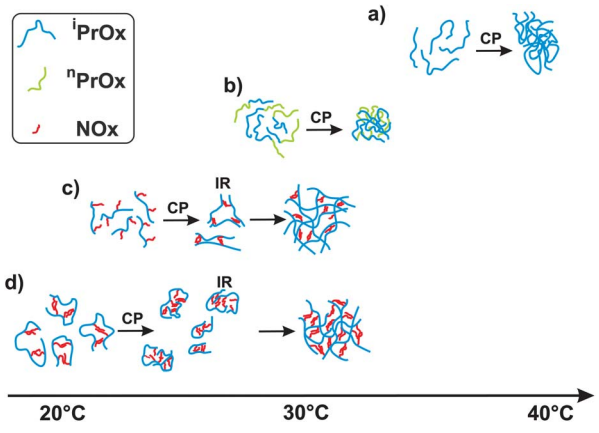

Fig. 12 Temperature-dependent aggregation behaviour of (a) P(^{i}PrOx) homopolymers, (b) P(^{i}PrOx$_{25}$-*b*-^{n}PrOx$_{25}$) diblock copolymers, (c) P[^{i}PrOx$_{48}$NOx$_{2}$]$_{grad}$, and (d) P[^{i}PrOx$_{46}$NOx$_{4}$]$_{grad}$ gradient copolymers. The different colours indicate the monomer type. CP stands for cloud point, IR for the intermediate regime. (Adapted from Salzinger *et al.*[182])

At the cloud point (above 40 °C for P(^{i}PrOx) and 24–38 °C for P(^{n}PrOx)) the polymer chains collapsed and formed large aggregates (Fig. 12a). Aggregation was fully reversible for P(^{i}PrOx) whereas the aggregates of P(^{n}PrOx) could not be fully dissolved upon cooling. The latter fact was tentatively attributed to crystallization of the *n*-propyl side-chains occurring above the cloud point. The aggregation of the copolymers with a P^{i}PrOx and a P^{n}PrOx block was dominated by the behaviour of P^{n}PrOx, the block with the lower cloud point. At this point, aggregates formed directly (Fig. 12b), in contrast to the expectation that micelles appear at temperatures between the cloud points of both polymers.

Apart from the homopolymers and the block copolymers, the authors also studied gradient copolymers, in which, on average, 2 or 4 out of 50 iso-propyl side groups were replaced by the very hydrophobic *n*-nonyl side group. These gradient copolymers displayed a complex aggregation behaviour resulting from the interplay between intra- and intermolecular association mediated by the hydrophobic ^{n}PrOx side chains. Already below the cloud point, aggregates are formed due to the strong interaction of the strongly hydrophobic *n*-nonyl side groups (Fig. 12c and d). This effect was more pronounced for the gradient copolymers with a higher number of *n*-nonyl side groups. The hydrophobic interaction of these groups also shifts the collapse resulting in large aggregates to a few Kelvin above the cloud point. These aggregates, however could not be detected with FCS, because sedimentation occurred due to their large size.

The size of unimers and aggregates of random amphiphilic copolymers was determined using a combination of FCS and electron paramagnetic resonance spectroscopy (EPR).[184] The percentage of hydrophobic monomers in the polymers was found to determine their shape and also their capability to bind the drug domperidone. Only if the content of apolar monomers is sufficiently high to form hydrophobic microdomains, the model drug can be solubilized, thus increasing the radius of the aggregates as determined by FCS. FCS is not only restricted to assembly studies of block copolymers and homopolymers, but also more complex aggregation systems can be analysed. As an example, Štěpánek *et al.* investigated the solution behaviour and self-assembly of a heteroarm star copolymer consisting of *ca.* 20 short PS and 20 long P2VP arms.[185]

Comparison of FCS with DLS and quasielastic neutron scattering (QENS)

Apart from FCS, dynamic light scattering (DLS, also known as photon correlation spectroscopy) is an often used method to investigate the dynamics of particles, micelles and aggregates. Thus, the question arises how these two techniques compare to each other. FCS requires tiny amounts of fluorescence probes reporting on their dynamics. The amount of probes is approx. 3–4 magnitudes lower than the one required for DLS. Therefore, the amount of those probes which are bound to micelles and aggregates is also typically not very high. This bears the big advantage that simultaneous detection of free dye, micelles and large aggregates is straight-forward. In contrast to that, the

scattered intensity detected in DLS is proportional to the particle mass and concentration.[185] Thus, small aggregates are difficult to detect in the presence of large aggregates.[177] FCS is also more sensitive to measure the hydrodynamic radius of nanoparticles.[41] Another important difference arises when probing polydisperse particles, micelles or aggregates. The value measured with FCS is a number-averaged molar mass (M_n) whereas the weight-averaged molar mass (M_w) is obtained during DLS measurements.[180]

Another very useful and well-established technique to study the dynamics of polymer systems is quasielastic neutron scattering (QENS) which can access diffusional processes at sub-nanometer length and picosecond time scales, *i.e.* with clearly higher accuracy than optical techniques, without the need of labelling.[186] However, due to the low cross-section of QENS which is *ca.* 10^9 times smaller than the absorption cross-section of a good fluorophore (*ca.* 10^{-28} m^2 *versus ca.* 10^{-19} m^2), it requires long measuring times of hours and averaging of a large ensemble of molecules to obtain a sufficient statistics, and thus imaging different sample areas would be very time-consuming and expensive. In addition, due to the limited availability of neutron sources, QENS will be never considered as a technique which can as routinely be used as FCS. However, I see a huge potential of combining the different techniques to gain the maximum insight into polymer structure and dynamics.

Conclusions

This review intended to present the studies performed to investigate structure and dynamics in polymer systems using fluorescence correlation spectroscopy. It outlined the capabilities and strengths, but also the pitfalls for FCS measurements in polymer science, illustrated by numerous references. In particular, it was focused on diffusion of differently sized molecular and macromolecular probes in polymer solutions, classical and responsive polymer gels, polymer melts, glasses, and micellization and aggregation systems. The observation of diffusional processes in these systems with the temporal and spatial resolution of FCS enables access to plenty of structural and dynamical parameters. This knowledge is essential for experimental and theoretical polymer scientists in order to gain a better understanding of how the structure and dynamics on the nano- to micrometre scale determine the macroscopic properties of polymers. As a final conclusion, I want to emphasize that FCS must be considered a powerful technique complementing other methods in polymer science.

Abbreviations

2fFCS	Dual-focus fluorescence correlation spectroscopy
APD	Avalanche photodiode
CAC	Critical aggregation concentration
CMC	Critical micelle concentration
DLS	Dynamic light scattering
FCCS	Fluorescence cross correlation spectroscopy
FCS	Fluorescence correlation spectroscopy
fcFCS	Full correlation FCS
LCST	Lower critical solution temperature
M_w	Weight-averaged molecular weight
M_n	Number-averaged molecular weight
NOx	2-*n*-Nonyl-2-oxazoline
ORB	Octadecyl rhodamine B
P2VP	Poly(2-vinylpyridine)
PDMS	Polydimethylsiloxane
PEG	Polyethylene glycol
PFG-NMR	Pulsed-field-gradient nuclear magnetic resonance
PMA	Poly(methyl acrylate)
PMAA	Polymethacrylic acid
PNIPAM	Poly(*N*-isopropylacrylamide), (PNIPAAm, PNIPA)
^{i}PrOx	2-Iso-propyl-2-oxazoline
^{n}PrOx	2-*n*-Propyl-2-oxazoline
PS	Polystyrene
PVA	Polyvinyl alcohol
QENS	Quasielastic neutron scattering
Rh6G	Rhodamine 6G
RhB	Rhodamine B
TIR-FCS	Total internal reflection FCS

Acknowledgements

The author thanks the Zukunftskolleg of the University of Konstanz for financial and administrative support.

Notes and references

1 D. Magde, W. W. Webb and E. Elson, *Phys. Rev. Lett.*, 1972, **29**, 705–708.
2 *Fluorescence Correlation Spectroscopy. Theory and Applications*, ed. R. Rigler and E. L. Elson, Springer-Verlag, Berlin, Heidelberg, New York, 2001.
3 P. Schwille, *Cell Biochem. Biophys.*, 2001, **34**, 383–408.
4 O. Krichevsky and G. Bonnet, *Rep. Prog. Phys.*, 2002, **65**, 251–297.
5 E. Haustein and P. Schwille, *Annu. Rev. Biophys. Biomol. Struct.*, 2007, **36**, 151–169.
6 E. L. Elson, *Biophys. J.*, 2011, **101**, 2855–2870.
7 M. Sauer, J. Hofkens and J. Enderlein, *Handbook of Fluorescence Spectroscopy and Imaging – From Single Molecules to Ensembles*, Wiley-VCH, Weinheim, 2011.
8 R. Rigler, Ü. Mets, J. Widengren and P. Kask, *Eur. Biophys. J.*, 1993, **22**, 169–175.
9 R. Shusterman, S. Alon, T. Gavrinyov and O. Krichevsky, *Phys. Rev. Lett.*, 2004, **92**, 048303.
10 E. P. Petrov, T. Ohrt, R. G. Winkler and P. Schwille, *Phys. Rev. Lett.*, 2006, **97**, 258101.
11 R. Shusterman, T. Gavrinyov and O. Krichevsky, *Phys. Rev. Lett.*, 2008, **100**, 098102.
12 D. Lumma, S. Keller, T. Vilgis and J. O. Rädler, *Phys. Rev. Lett.*, 2003, **90**, 218301.
13 R. G. Winkler, S. Keller and J. O. Rädler, *Phys. Rev. E: Stat., Nonlinear, Soft Matter Phys.*, 2006, **73**, 041919.

14 M. Kinjo and R. Rigler, *Nucleic Acids Res.*, 1995, **23**, 1795–1799.
15 P. Schwille, F. J. Meyer-Almes and R. Rigler, *Biophys. J.*, 1997, **72**, 1878–1886.
16 X. Chen, Y. Zhou, P. Qu and X. S. Zhao, *J. Am. Chem. Soc.*, 2008, **130**, 16947–16952.
17 S. John Bosco, H. Zettl, J. J. Crassous, M. Ballauff and G. Krausch, *Macromolecules*, 2006, **39**, 8793–8798.
18 H. Park and K. Y. Lee, *Soft Matter*, 2011, **7**, 4876–4880.
19 L. Yang and L.-M. Zhang, *Carbohydr. Polym.*, 2009, **76**, 349–361.
20 D. S. Banks and C. Fradin, *Biophys. J.*, 2005, **89**, 2960–2971.
21 S. P. Zustiak, R. Nossal and D. L. Sackett, *Biophys. J.*, 2011, **101**, 255–264.
22 R. Rigler, A. Pramanik, P. Jonasson, G. Kratz, O. T. Jansson, P. A. Nygren, S. Stahl, K. Ekberg, B. L. Johansson, S. Uhlen, M. Uhlen, H. Jornvall and J. Wahren, *Proc. Natl. Acad. Sci. U. S. A.*, 1999, **96**, 13318–13323.
23 N. Baudendistel, G. Müller, W. Waldeck, P. Angel and J. Langowski, *ChemPhysChem*, 2005, **6**, 984–990.
24 L. Rusu, A. Gambhir, S. McLaughlin and J. Rädler, *Biophys. J.*, 2004, **87**, 1044–1053.
25 J. Widengren, Ü. Mets and R. Rigler, *Chem. Phys.*, 1999, **250**, 171–186.
26 K. Chattopadhyay, E. L. Elson and C. Frieden, *Proc. Natl. Acad. Sci. U. S. A.*, 2005, **102**, 2385–2389.
27 H. Neuweiler, M. Löllmann, S. Doose and M. Sauer, *J. Mol. Biol.*, 2007, **365**, 856–869.
28 S. L. Crick, M. Jayaraman, C. Frieden, R. Wetzel and R. V. Pappu, *Proc. Natl. Acad. Sci. U. S. A.*, 2006, **103**, 16764–16769.
29 A. Bernheim-Groswasser, R. Shusterman and O. Krichevsky, *J. Chem. Phys.*, 2006, **125**, 084903.
30 J. Borejdo, *Biopolymers*, 1979, **18**, 2807–2820.
31 N. Bark, Z. Foldes-Papp and R. Rigler, *Biochem. Biophys. Res. Commun.*, 1999, **260**, 35–41.
32 C. Eggeling, P. Kask, D. Winkler and S. Jäger, *Biophys. J.*, 2005, **89**, 605–618.
33 K. Salamon, D. Aumiler, G. Pabst and T. Vulerić, *Macromolecules*, 2013, **46**, 1107–1118.
34 G. Pembouong, N. Morellet, T. Kral, M. Hof, D. Scherman, M.-F. Bureau and N. Mignet, *J. Controlled Release*, 2011, **151**, 57–64.
35 H. Lin, Y. Tian, K. Zapadka, G. Persson, D. Thomsson, O. Mirzov, P.-O. Larsson, J. Widengren and I. G. Scheblykin, *Nano Lett.*, 2009, **9**, 4456–4461.
36 D. Wang, L. Pevzner, C. Li, K. Peneva, C. Y. Li, D. Y. C. Chan, K. Müllen, M. Mezger, K. Koynov and H.-J. Butt, *Phys. Rev. E: Stat., Nonlinear, Soft Matter Phys.*, 2013, **87**, 012403.
37 C. R. Daniels, C. Reznik and C. F. Landes, *Langmuir*, 2010, **26**, 4807–4812.
38 K. Starchev, J. Buffle and E. Pérez, *J. Colloid Interface Sci.*, 1999, **213**, 479–487.
39 K. Starchev, J. Zhang and J. Buffle, *J. Colloid Interface Sci.*, 1998, **203**, 189–196.
40 J. J. Zhao, S. C. Bae, F. Xie and S. Granick, *Macromolecules*, 2001, **34**, 3123–3126.
41 P. Jurkiewicz, Č. Koňák, V. Šubr, M. Hof, P. Štěpánek and K. Ulbrich, *Macromol. Chem. Phys.*, 2008, **209**, 1447–1453.
42 D. Schaeffel, R. H. Staff, H.-J. Butt, K. Landfester, D. Crespy and K. Koynov, *Nano Lett.*, 2012, **12**, 6012–6017.
43 T. Pellegrino, L. Manna, S. Kudera, T. Liedl, D. Koktysh, A. L. Rogach, S. Keller, J. Rädler, G. Natile and W. J. Parak, *Nano Lett.*, 2004, **4**, 703–707.
44 K. Kang, J. Gapinski, M. P. Lettinga, J. Buitenhuis, G. Meier, M. Ratajczyk, J. K. G. Dhont and A. Patkowski, *J. Chem. Phys.*, 2005, **122**, 044905.
45 K. Koynov and H.-J. Butt, *Curr. Opin. Colloid Interface Sci.*, 2012, **17**, 377–387.
46 C. B. Müller, A. Loman, V. Pacheco, F. Koberling, D. Willbold, W. Richtering and J. Enderlein, *Europhys. Lett.*, 2008, **83**, 46001.
47 J. Enderlein, *Phys. Rev. Lett.*, 2012, **108**, 108101.
48 O. Krichevsky, *Phys. Rev. Lett.*, 2013, **110**, 159801.
49 F. Höfling, K. U. Bamberg and T. Franosch, *Soft Matter*, 2011, **7**, 1358–1363.
50 N. L. Thompson, in *Topics in Fluorescence Spectroscopy*, ed. J. R. Lakowicz, Plenum Press, New York, 1991, vol. 1, pp. 337–410.
51 Y. Chen, J. D. Müller, K. M. Berland and E. Gratton, *Methods*, 1999, **19**, 234–252.
52 S. W. Provencher, *Makromol. Chem.*, 1979, **180**, 201–209.
53 S. W. Provencher, *Comput. Phys. Commun.*, 1982, **27**, 213–227.
54 S. W. Provencher, *Comput. Phys. Commun.*, 1982, **27**, 229–242.
55 P. Sengupta, K. Garai, J. Balaji, N. Periasamy and S. Maiti, *Biophys. J.*, 2003, **84**, 1977–1984.
56 U. Zettl, S. T. Hoffmann, F. Koberling, G. Krausch, J. Enderlein, L. Harnau and M. Ballauff, *Macromolecules*, 2009, **42**, 9537–9547.
57 T. Cherdhirankorn, G. Floudas, H.-J. Butt and K. Koynov, *Macromolecules*, 2009, **42**, 9183–9189.
58 M. Weiss, M. Elsner, F. Kartberg and T. Nilsson, *Biophys. J.*, 2004, **87**, 3518–3524.
59 M. Wachsmuth, W. Waldeck and J. Langowski, *J. Mol. Biol.*, 2000, **298**, 677–689.
60 A. Masuda, K. Ushida and T. Okamoto, *Phys. Rev. E: Stat., Nonlinear, Soft Matter Phys.*, 2005, **72**, 060101.
61 N. K. Reitan, A. Juthajan, T. Lindmo and C. de Lange Davies, *J. Biomed. Opt.*, 2008, **13**, 054040.
62 M. J. Saxton, *Biophys. J.*, 1995, **69**, 389–398.
63 N. Fatin-Rouge, K. Starchev and J. Buffle, *Biophys. J.*, 2004, **86**, 2710–2719.
64 M. Weiss, H. Hashimoto and T. Nilsson, *Biophys. J.*, 2003, **84**, 4043–4052.
65 A. Masuda, K. Ushida and T. Okamoto, *J. Photochem. Photobiol., A*, 2006, **183**, 304–308.
66 A. Masuda, K. Ushida and T. Okamoto, *Biophys. J.*, 2005, **88**, 3584–3591.
67 J. Enderlein, I. Gregor, D. Patra, T. Dertinger and U. B. Kaupp, *ChemPhysChem*, 2005, **6**, 2324–2336.
68 P. Košovan, F. Uhlík, J. Kuldová, M. Štěpánek, Z. Limpouchová, K. Procházka, A. Benda, J. Humpolíčková

and M. Hof, *Collect. Czech. Chem. Commun.*, 2011, **76**, 207–222.
69 A. Vagias, R. Raccis, K. Koynov, U. Jonas, H.-J. Butt, G. Fytas, P. Košovan, O. Lenz and C. Holm, *Phys. Rev. Lett.*, 2013, **111**, 088301.
70 P. Kask, P. Piksarv, Ü. Mets, M. Pooga and E. Lippmaa, *Eur. Biophys. J.*, 1987, **14**, 257–261.
71 M. Dorfschmid, K. Müllen, A. Zumbusch and D. Wöll, *Macromolecules*, 2010, **43**, 6174–6179.
72 A. Loman, I. Gregor, C. Stutz, M. Mund and J. Enderlein, *Photochem. Photobiol. Sci.*, 2010, **2010**, 627–636.
73 C. M. Pieper and J. Enderlein, *Chem. Phys. Lett.*, 2011, **516**, 1–11.
74 J. M. Tsay, S. Doose and S. Weiss, *J. Am. Chem. Soc.*, 2006, **128**, 1639–1647.
75 M. Ehrenberg and R. Rigler, *Chem. Phys.*, 1974, **4**, 390–401.
76 S. R. Aragón and R. Pecora, *Biopolymers*, 1975, **14**, 119–137.
77 S. R. Aragón and R. Pecora, *J. Chem. Phys.*, 1976, **64**, 1791–1803.
78 R. Hanbury Brown and R. Q. Twiss, *Nature*, 1956, **177**, 27–29.
79 S. Felekyan, R. Kühnemuth, V. Kudryavtsev, C. Sandhagen, W. Becker and C. A. M. Seidel, *Rev. Sci. Instrum.*, 2005, **76**, 083104.
80 M. Wahl, H.-J. Rahn, I. Gregor, R. Erdmann and J. Enderlein, *Rev. Sci. Instrum.*, 2007, **78**, 033106.
81 T. Dertinger, V. Pacheco, I. von der Hocht, R. Hartmann, I. Gregor and J. Enderlein, *ChemPhysChem*, 2007, **8**, 433–443.
82 C. B. Müller, K. Weiss, A. Loman, J. Enderlein and W. Richtering, *Lab Chip*, 2009, **9**, 1248–1253.
83 C. B. Müller, T. Eckert, A. Loman, J. Enderlein and W. Richtering, *Soft Matter*, 2009, **5**, 1358–1366.
84 N. Pal, S. D. Verma, M. K. Singh and S. Sen, *Anal. Chem.*, 2011, **83**, 7736–7744.
85 T. Dertinger, A. Loman, B. Ewers, C. B. Müller, B. Kramer and J. Enderlein, *Opt. Express*, 2008, **16**, 14353–14368.
86 C. B. Müller, A. Loman, W. Richtering and J. Enderlein, *J. Phys. Chem. B*, 2008, **112**, 8236–8240.
87 N. L. Thompson, T. P. Burghardt and D. Axelrod, *Biophys. J.*, 1981, **33**, 435–454.
88 S. Yordanov, A. Best, H.-J. Butt and K. Koynov, *Opt. Express*, 2009, **17**, 21149–21158.
89 S. Yordanov, A. Best, K. Weisshart and K. Koynov, *Rev. Sci. Instrum.*, 2011, **82**, 036105.
90 N. L. Thompson, X. Wang and P. Navaratnarajah, *J. Struct. Biol.*, 2009, **168**, 95–106.
91 D. Ivanov, V. Shcheslavskiy, I. Marki, M. Leutenegger and T. Lasser, *Appl. Phys. Lett.*, 2009, **94**, 083902–083903.
92 L. Kastrup, H. Blom, C. Eggeling and S. W. Hell, *Phys. Rev. Lett.*, 2005, **94**, 178104.
93 C. Eggeling, C. Ringemann, R. Medda, G. Schwarzmann, K. Sandhoff, S. Polyakova, V. N. Belov, B. Hein, C. von Middendorff, A. Schonle and S. W. Hell, *Nature*, 2009, **457**, 1159–1162.
94 P. Schwille, U. Haupts, S. Maiti and W. W. Webb, *Biophys. J.*, 1999, **77**, 2251–2265.
95 C. Grabowski and A. Mukhopadhyay, *Macromolecules*, 2008, **41**, 6191–6194.
96 S. A. Sukhishvili, Y. Chen, J. D. Müller, E. Gratton, K. S. Schweizer and S. Granick, *Macromolecules*, 2002, **35**, 1776–1784.
97 K. M. Berland, P. T. So and E. Gratton, *Biophys. J.*, 1995, **68**, 694–701.
98 P. S. Dittrich and P. Schwille, *Anal. Chem.*, 2002, **74**, 4472–4479.
99 W. Kügel, A. Muschielok and J. Michaelis, *ChemPhysChem*, 2012, **13**, 1013–1022.
100 W. K. Ridgeway, D. P. Millar and J. R. Williamson, *J. Phys. Chem. B*, 2012, **116**, 1908–1919.
101 S. Felekyan, S. Kalinin, H. Sanabria, A. Valeri and C. A. Seidel, *ChemPhysChem*, 2012, **13**, 1036–1053.
102 R. Kühnemuth and C. A. M. Seidel, *Single Mol.*, 2001, **2**, 251–254.
103 A. Schob, F. Cichos, J. Schuster and C. von Borczyskowski, *Eur. Polym. J.*, 2004, **40**, 1019–1026.
104 C. B. Müller and W. Richtering, *Colloid Polym. Sci.*, 2008, **286**, 1215–1222.
105 B. M. I. Flier, M. C. Baier, J. Huber, K. Müllen, S. Mecking, A. Zumbusch and D. Wöll, *J. Am. Chem. Soc.*, 2012, **134**, 480–488.
106 S. T. Hess and W. W. Webb, *Biophys. J.*, 2002, **83**, 2300–2317.
107 S. Hell, G. Reiner, C. Cremer and E. H. K. Stelzer, *J. Microsc.*, 1993, **169**, 391–405.
108 J. Enderlein, I. Gregor, D. Patra and J. Fitter, *Curr. Pharm. Biotechnol.*, 2004, **5**, 155–161.
109 H. Zettl, W. Häfner, A. Böker, H. Schmalz, M. Lanzendorfer, A. H. E. Müller and G. Krausch, *Macromolecules*, 2004, **37**, 1917–1920.
110 H. Zettl, U. Zettl, G. Krausch, J. Enderlein and M. Ballauff, *Phys. Rev. E: Stat., Nonlinear, Soft Matter Phys.*, 2007, **75**, 061804.
111 K. Koynov, G. Mihov, M. Mondeshki, C. Moon, H. W. Spiess, K. Müllen, H. J. Butt and G. Floudas, *Biomacromolecules*, 2007, **8**, 1745–1750.
112 W. Wang, C. Zhang, S. Wang and J. Zhao, *Macromolecules*, 2007, **40**, 9564–9569.
113 R. G. Liu, X. Gao, J. Adams and W. Oppermann, *Macromolecules*, 2005, **38**, 8845–8849.
114 A. Tcherniak, C. Reznik, S. Link and C. F. Landes, *Anal. Chem.*, 2009, **81**, 746–754.
115 J. Widengren, R. Rigler and Ü. Mets, *J. Fluoresc.*, 1994, **4**, 255–258.
116 L. M. Davis and G. Shen, *Curr. Pharm. Biotechnol.*, 2006, **7**, 287–301.
117 J. Widengren, Ü. Mets and R. Rigler, *J. Phys. Chem.*, 1995, **99**, 13368–13379.
118 A. V. R. Murthy, M. Goel, S. Patil and M. Jayakannan, *J. Phys. Chem. B*, 2011, **115**, 10779–10788.
119 R. G. Winkler, *J. Chem. Phys.*, 2007, **127**, 054904.
120 W. W. Graessley, *Polymer*, 1980, **21**, 258–262.
121 J. J. Magda and S. G. Baek, *Polymer*, 1994, **35**, 1187–1194.

122 J. Won, C. Onyenemezu, W. G. Miller and T. P. Lodge, *Macromolecules*, 1994, **27**, 7389–7396.
123 X. Ye, P. Tong and L. J. Fetters, *Macromolecules*, 1998, **31**, 5785–5793.
124 R. Holyst, A. Bielejewska, J. Szymanski, A. Wilk, A. Patkowski, J. Gapinski, A. Zywocinski, T. Kalwarczyk, E. Kalwarczyk, M. Tabaka, N. Ziebacz and S. A. Wieczorek, *Phys. Chem. Chem. Phys.*, 2009, **11**, 9025–9032.
125 A. Michelman-Ribeiro, F. Horkay, R. Nossal and H. Boukari, *Biomacromolecules*, 2007, **8**, 1595–1600.
126 R. A. Omari, A. M. Aneese, C. A. Grabowski and A. Mukhopadhyay, *J. Phys. Chem. B*, 2009, **113**, 8449–8452.
127 G. D. J. Phillies, *J. Phys. Chem.*, 1989, **93**, 5029–5039.
128 H. Fujita, *Fortschr. Hochpolym.-Forsch.*, 1961, **3**, 1–47.
129 J. S. Vrentas and J. L. Duda, *J. Polym. Sci., Polym. Lett. Ed.*, 1977, **15**, 403–416.
130 J. M. Petit, B. Roux, X. X. Zhu and P. M. Macdonald, *Macromolecules*, 1996, **29**, 6031–6036.
131 G. Modesti, B. Zimmermann, M. Börsch, A. Herrmann and K. Saalwächter, *Macromolecules*, 2009, **42**, 4681–4689.
132 T. Cherdhirankorn, A. Best, K. Koynov, K. Peneva, K. Müllen and G. Fytas, *J. Phys. Chem. B*, 2009, **113**, 3355–3359.
133 A. Best, T. Pakula and G. Fytas, *Macromolecules*, 2005, **38**, 4539–4541.
134 T. Cherdhirankorn, V. Harmandaris, A. Juhari, P. Voudouris, G. Fytas, K. Kremer and K. Koynov, *Macromolecules*, 2009, **42**, 4858–4866.
135 M. Doroshenko, M. Gonzales, A. Best, H.-J. Butt, K. Koynov and G. Floudas, *Macromol. Rapid Commun.*, 2012, **33**, 1568–1573.
136 A. Michelman-Ribeiro, H. Boukari, R. Nossal and F. Horkay, *Macromolecules*, 2004, **37**, 10212–10214.
137 R. Raccis, R. Roskamp, I. Hopp, B. Menges, K. Koynov, U. Jonas, W. Knoll, H. J. Butt and G. Fytas, *Soft Matter*, 2011, **7**, 7042–7053.
138 S. P. Zustiak, H. Boukari and J. B. Leach, *Soft Matter*, 2010, **6**, 3609–3618.
139 R. Zhang, T. Cherdhirankorn, K. Graf, K. Koynov and R. Berger, *Microelectron. Eng.*, 2008, **85**, 1261–1264.
140 D. Wöll, H. Uji-i, T. Schnitzler, J. Hotta, P. Dedecker, A. Herrmann, F. C. De Schryver, K. Müllen and J. Hofkens, *Angew. Chem., Int. Ed.*, 2008, **47**, 783–787.
141 N. Ide and T. Fukuda, *Macromolecules*, 1999, **32**, 95–99.
142 B. Stempfle, M. Dill, M. J. Winterhalder, K. Müllen and D. Wöll, *Polym. Chem.*, 2012, **3**, 2456–2463.
143 J. G. Kirkwood and J. Riseman, *J. Chem. Phys.*, 1948, **16**, 565–573.
144 P.-G. de Gennes, *Scaling Concepts in Polymer Physics*, Cornell University Press, London, 1979.
145 W. Hess, *Macromolecules*, 1986, **19**, 1395–1404.
146 M. Doi and D. A. Edwards, *The Theory of Polymer Dynamics*, Oxford University Press, New York, 1986.
147 J. S. Vrentas and J. L. Duda, *J. Polym. Sci., Polym. Lett. Ed.*, 1977, **15**, 417–439.
148 U. Zettl, M. Ballauff and L. Harnau, *J. Phys.: Condens. Matter*, 2010, **22**, 494111.
149 D. Pristinski, V. Kozlovskaya and S. A. Sukhishvili, *J. Chem. Phys.*, 2005, **122**, 014907.
150 E. van Rompaey, Y. Engelborghs, N. Sanders, C. De Smedt and J. Demeester, *Pharm. Res.*, 2001, **18**, 928–936.
151 P. Jia, Q. Yang, Y. Gong and J. Zhao, *J. Chem. Phys.*, 2012, **136**, 084904.
152 B.-S. Kim, O. V. Lebedeva, K. Koynov, H. Gong, G. Glasser, I. Lieberwith and O. I. Vinogradova, *Macromolecules*, 2005, **38**, 5214–5222.
153 M. Orrit, *Angew. Chem., Int. Ed.*, 2013, **52**, 163–166.
154 A. Casoli and M. Schönhoff, *Biol. Chem.*, 2001, **382**, 363–369.
155 S. Rathgeber, H. J. Beauvisage, H. Chevreau, N. Willenbacher and C. Oelschlaeger, *Langmuir*, 2009, **25**, 6368–6376.
156 M. J. Solomon and Q. Lu, *Curr. Opin. Colloid Interface Sci.*, 2001, **6**, 430–437.
157 L. Joly, C. Ybert and L. Bocquet, *Phys. Rev. Lett.*, 2006, **96**, 046101.
158 C. Wu and X. Wang, *Phys. Rev. Lett.*, 1998, **80**, 4092–4094.
159 M. Gianneli, P. W. Beines, R. F. Roskamp, K. Koynov, G. Fytas and W. Knoll, *J. Phys. Chem. C*, 2007, **111**, 13205–13211.
160 B. Ferse, S. Richter, F. Eckert, A. Kulkarni, C. M. Papadakis and K. F. Arndt, *Langmuir*, 2008, **24**, 12627–12635.
161 M. A. Hink, R. A. Griep, J. W. Borst, A. van Hoek, M. H. M. Eppink, A. Schots and A. J. W. G. Visser, *J. Biol. Chem.*, 2000, **275**, 17556–17560.
162 S. Lehmann, S. Seiffert and W. Richtering, *J. Am. Chem. Soc.*, 2012, **134**, 15963–15969.
163 J. E. Wong, C. B. Müller, A. Laschewsky and W. Richtering, *J. Phys. Chem. B*, 2007, **111**, 8527–8531.
164 J. E. Wong, C. B. Müller, A. M. Diez-Pascual and W. Richtering, *J. Phys. Chem. B*, 2009, **113**, 15907–15913.
165 C. H. Hofmann, F. A. Plamper, C. Scherzinger, S. Hietala and W. Richtering, *Macromolecules*, 2012, **46**, 523–532.
166 F. Wang, Y. Shi, S. Luo, Y. Chen and J. Zhao, *Macromolecules*, 2012, **45**, 9196–9204.
167 P. J. Flory, *Principles of Polymer Chemistry*, Cornell University Press, 1953.
168 S. A. Sukhishvili, Y. Chen, J. D. Müller, E. Gratton, K. S. Schweizer and S. Granick, *Nature*, 2000, **406**, 146.
169 J. Zhao and S. Granick, *J. Am. Chem. Soc.*, 2004, **126**, 6242–6243.
170 J. Zhao and S. Granick, *Macromolecules*, 2007, **40**, 1243–1247.
171 X. Pan, C. Aw, Y. Du, H. Yu and T. Wohland, *Biophys. Rev. Lett.*, 2006, **1**, 1–9.
172 C. Reznik, N. Estillore, R. C. Advincula and C. F. Landes, *J. Phys. Chem. B*, 2009, **113**, 14611–14618.
173 M. A. Hink, A. van Hoek and A. J. W. G. Visser, *Langmuir*, 1999, **15**, 992–997.
174 K. Loos, A. Böker, H. Zettl, M. Zhang, G. Krausch and A. H. E. Müller, *Macromolecules*, 2005, **38**, 873–879.
175 R. Nörenberg, J. Klingler and D. Horn, *Angew. Chem., Int. Ed.*, 1999, **38**, 1626–1629.

176 H. Schuch, J. Klingler, P. Rossmanith, T. Frechen, M. Gerst, J. Feldthusen and A. H. E. Müller, *Macromolecules*, 2000, **33**, 1734–1740.
177 T. B. Bonné, K. Ludtke, R. Jordan, P. Stepanek and C. M. Papadakis, *Colloid Polym. Sci.*, 2004, **282**, 1425.
178 T. B. Bonné, C. M. Papadakis, K. Ludtke and R. Jordan, *Colloid Polym. Sci.*, 2007, **285**, 491–497.
179 O. Colombani, M. Ruppel, F. Schubert, H. Zettl, D. V. Pergushov and A. H. E. Müller, *Macromolecules*, 2007, **40**, 4338–4350.
180 J. Humpolíčková, K. Procházka, M. Hof, Z. Tuzar and M. Špírková, *Langmuir*, 2003, **19**, 4111–4119.
181 O. Sedlacek, B. D. Monnery, S. K. Filippov, R. Hoogenboom and M. Hruby, *Macromol. Rapid Commun.*, 2012, **33**, 1648–1662.
182 S. Salzinger, S. Huber, S. Jaksch, P. Busch, R. Jordan and C. M. Papadakis, *Colloid Polym. Sci.*, 2012, **290**, 385–400.
183 Y. Okada and F. Tanaka, *Macromolecules*, 2005, **38**, 4465–4471.
184 M. Hemmelmann, D. Kurzbach, K. Koynov, D. Hinderberger and R. Zentel, *Biomacromolecules*, 2012, **13**, 4065–4074.
185 M. Štěpánek, P. Matějíček, J. Humpolíčková, J. Havránkovaá, K. Podhájecká, M. Špírková, Z. Tuzar, C. Tsitsilianis and K. Procházka, *Polymer*, 2005, **46**, 10493–10505.
186 R. J. Roe, *Methods of X-Ray and Neutron Scattering in Polymer Science (Topics in Polymer Science)*, Oxford University Press, Inc., New York, 2000.